NASA TECHNICAL NOTE

NASA TN D-7854

NASA TN D-7854

RESULTS OF INDUCED ATMOSPHERE MEASUREMENTS FROM THE APOLLO PROGRAM

by Robert J. Naumann

George C. Marshall Space Flight Center

Marshall Space Flight Center, Ala. 35812

NATIONAL AERONAUTICS AND SPACE ADMINISTRATION • WASHINGTON, D. C. • DECEMBER 1974

TECHNICAL REPORT STANDARD TITLE PAGE

1. REPORT NO.	2. GOVERNMENT ACCESSION NO.	3. RECIPIENT'S CATALOG NO.
TN D-7854		

4. TITLE AND SUBTITLE	5. REPORT DATE
Results of Induced Atmosphere Measurements from the Apollo Program	December 1974
	6. PERFORMING ORGANIZATION CODE

7. AUTHOR(S)	8. PERFORMING ORGANIZATION REPORT #
Robert J. Naumann	M464

9. PERFORMING ORGANIZATION NAME AND ADDRESS	10. WORK UNIT NO.
George C. Marshall Space Flight Center Marshall Space Flight Center, Alabama 35812	11. CONTRACT OR GRANT NO.
	13. TYPE OF REPORT & PERIOD COVERED
12. SPONSORING AGENCY NAME AND ADDRESS	
National Aeronautics and Space Administration Washington, D.C. 20546	Technical Note
	14. SPONSORING AGENCY CODE

15. SUPPLEMENTARY NOTES

Prepared by Space Sciences Laboratory, Science and Engineering

16. ABSTRACT

Because of concern about the possible effects of the induced environment in the vicinity of manned spacecraft on sensitive experiments planned for the Skylab and future manned laboratories, attempts were made to utilize experiments on Apollo missions 15, 16, and 17 to learn as much as possible about this induced environment. Photographic sequences were used to obtain scattered light data from the spacecraft-generated particulates during quiescence periods and after liquid dumps. The results allowed estimates of the obscuration factor (average particle cross section times the column density) and the clearing times after dumps. It was found that the clearing times were substantially longer than anticipated because the dump nozzle continues to produce particles long after the flow is terminated.

The mass spectrometer detected a surprisingly high molecular flux in lunar orbit which was obviously induced by the spacecraft. It is shown that this is most likely caused by small ice crystals being continually produced in lunar orbit, probably as a result of the thawing of the ice cones produced by the waste dumps.

Other data from the ultraviolet spectrometer and the stellar camera are also analyzed, and estimated values or upper limits are placed on the total scattering background, the size and number of particles generated, the velocity range, and the column density.

17. KEY WORDS	18. DISTRIBUTION STATEMENT
	CAT. 30

19. SECURITY CLASSIF. (of this report)	20. SECURITY CLASSIF. (of this page)	21. NO. OF PAGES	22. PRICE
Unclassified	Unclassified	51	$4.25

TABLE OF CONTENTS

LIST OF ILLUSTRATIONS

LIST OF ILLUSTRATIONS (Concluded)

RESULTS OF INDUCED ATMOSPHERE MEASUREMENTS FROM THE APOLLO PROGRAM

INTRODUCTION

Since the beginning of manned space flight there has been concern about the problem of spacecraft contamination from the so-called induced atmosphere. Windows were observed to have become coated, many ice crystals were observed to float around the spacecraft, and astronauts reported they were able to see only the brightest stars. Attempts to observe dim-light phenomena such as zodiacal light, gegenschein, and faint star fields were successful only when performed in the shadow of the earth or moon. It soon became widely believed that spacecraft were surrounded by contamination clouds that were responsible for the aforementioned effects.

Of particular concern for Skylab with its Apollo Telescope Mount (ATM) solar observatory was the particulate scattering background. This problem was first analyzed in 1967 by Newkirk, who concluded that if the water vapor in the crew cabin gas leakage were completely converted to ice crystals, the background radiance of the contamination cloud would be intolerably high for the leakage rate of Gemini and barely tolerable for Apollo [1]. He did point out that the inability of the astronauts to see faint stars could not be attributed to the contamination cloud. Kovar, Kovar, and Bonner were more pessimistic in their 1969 analysis and concluded that even if they overestimated the leakage rate on Skylab by two orders of magnitude, coronal and inner zodiacal light measurements would be marginal at best [2].

These arguments were refuted by Buffalano and Grobman on the grounds that nucleation of escaping H_2O molecules would be limited by the number of collisions available to sizes on the order of 0.01 micron, which would produce negligible scattering [3]. There is still the problem of particles generated by other means such as waste dumps, paint or insulation flakes, and residual dust particles.

Because of these uncertainties as well as those pertaining to material depositing on spacecraft surfaces, an effort was made in 1971 to utilize available instrumentation on the remaining Apollo missions to investigate the contamination problem and, hopefully, reduce some of the uncertainties. This report is a summary of the investigation results.

PHOTOGRAPHIC EXPERIMENTS

All photographs from previous manned flights were examined for contamination effects. Typical shots of contaminated windows are illustrated in Figure 1. The pattern of material distribution on the window is along the flight direction. This material was

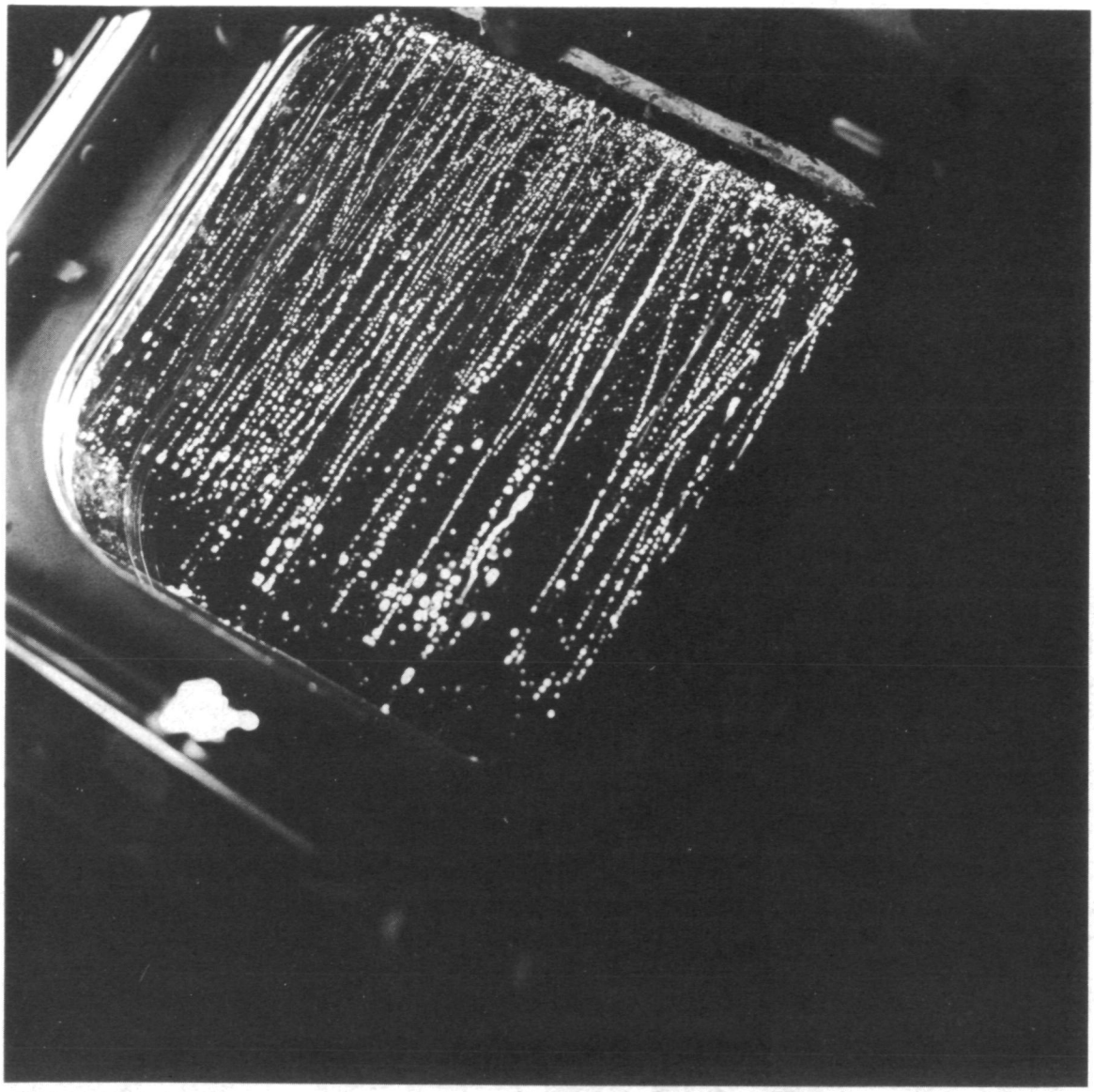

Figure 1. Apollo window photographed during flight. The deposits appear to be located between the inner and outer surface and are apparently viscous material that ran down the window during acceleration.

located between the panes and apparently originated from outgassing products of material in the region between the panes that collected and ran down the surface during the high g forces associated with launch. This situation was rectified on later flights.

A number of frames recorded particles resulting from overboard dumps. Unfortunately, these were not always taken in a controlled manner that allowed detailed scientific evaluation. Also, all dim-light photography of such phenomena as star fields, zodiacal light, and gegenschein had been taken in the umbra of the earth or moon to avoid any scattering from the spacecraft-induced atmosphere. It was desired to measure the scattered light background as a function of sun angle for a quiescent spacecraft. Further, it was desired to obtain data on the scattered light as a function of time after a waste dump to establish the clearing times required for the debris to disperse. Previous ground-based measurements of water releases from Apollo spacecraft yielded total brightness and cloud size as a function of time [4]. From these data an average particle size of ~500 microns (Appendix A) and an average velocity of 6 m/sec were estimated.

A sequence of star-field photographs was taken on Apollo 15 during trans-earth-coast when the spacecraft was approximately halfway between the earth and moon [5]. The spacecraft was oriented to prevent light from the sun and the earth from striking the window surface. A dark hood was used around the camera to prevent interior light from striking the window and reflecting into the camera. The camera was a 16-mm data acquisition camera with an 18-mm f/0.9 lens, focused at infinity. Type SO164 film (similar to Pan-x) was used. Exposures ranged from 1 sec to 100 sec to obtain a wide latitude.

The star field included m_v = 4.4 to 4.8 stars (g, h, i, and k Centaurus) which were easily identified. Stars as faint as m_v = 6.3 could be identified with some difficulty. The star images were measured to be 20 × 50 μ, primarily because of spacecraft motion during the long exposure times. A m_v = 6.3 star would be expected to produce a film density of 0.14 compared to a base fog of 0.06, assuming nominal transmission values of the window and lens. This is fairly consistent with the microdensitometer readings taken on the faintest stars; therefore, there does not seem to be any significant change in the windows. The Apollo 15 crew also reported that the windows remained clean during the mission. This was primarily because of an improved cure of the seal material between the window panes which had been responsible for the windows becoming coated in the earlier Apollo missions.

Some scattered light was evident in the star-field photographs (Fig. 2). It was impossible to orient the vehicle to exclude earth, moon, and sunlight completely from the window opening at the time the photographic sequence was taken. Moonlight was incident on the window opening but not directly on the window. Therefore, some of the observed background probably results from moonlight reflected or scattered from the window opening. Also, it is possible that some light leaked in through the dark hood in the region where the hood is drawn around the lens.

The background brightness in terms of solar brightness $B_{\odot}$ was inferred from film density using sensitometry data provided by the Johnson Space Center photolab. The sensitometry was obtained for the actual exposure times used to account for film reciprocity failure.

BEFORE DUMP

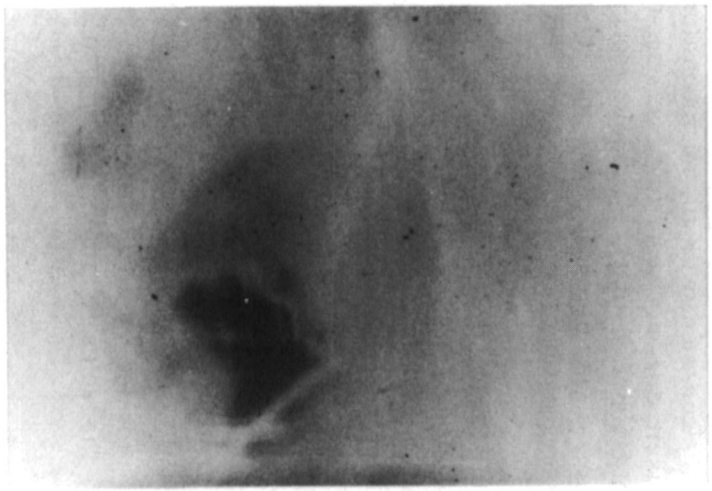

60 SECONDS

100 SECONDS

Figure 2. Apollo 15 star-field photographs taken at 60 sec and 100 sec at f/0.9 on S0164 film. Dark region at bottom and at left of center is scattered moonlight and internal light reflected from the CM window. Brightest stars are θ-Centauri (m_v = 2.3) top center, γ-Hydra (m_v = 3.3) left center, and π-Hydra (m_v = 3.5) center. The cluster of 4 stars near top center are h, i, j, k Centauri (m_v = 4.4 to 4.8). Several objects that resemble stars are visible on one frame but not on the other. Since the frames were taken in close sequence, these objects must be artifacts such as dust on the film. If they were ice crystals, they would appear as streaks because of their motion.

Assuming the nominal transmission for the windows did not change significantly during the flight, which the observation of threshold stars confirms, the worst case background brightness was $10^{-11.71}$ $B_{\odot}$ for a sun angle of 75 deg. However, this is almost certainly due to the aforementioned stray light. There were also regions where the measured film density was 0.06, which is the base fog value. This places an upper limit of $10^{-12.3}$ $B_{\odot}$ on the background brightness at a sun angle of 91 deg. This upper limit is set by film sensitivity (the very high speed 2485 film originally planned for this experiment was not available), scattered moonlight, or light leaks in the dark hood. This brightness is approximately a factor of 3 higher than a perfect sky (airglow + unresolved stars) and certainly would not prevent the astronaut from observing faint stars. It is lower than the Apollo environment estimated by Kovar, Kovar, and Bonner but slightly higher than the estimate of Newkirk. Assuming the particles have an albedo of near unity, an upper limit of 1.24×10^{-7} can be set for the obscuration fraction, defined as the product of the geometric cross section and the column density.

A similar sequence was attempted on Apollo 16 using the very high speed 2485 film and orienting the vehicle to obtain different sun angles. This effort was severely hampered by moonlight. The early return of Apollo 16, necessitated by problems with the thrust vector control, placed the spacecraft in such a position relative to the moon that it was impossible to prevent direct moonlight in the window opening. An additional problem was created by the fact that the spacecraft altitude had previously been held for a long period of time with the window portion shadowed. The low window temperatures resulted in moisture condensing on the inside surfaces.

The Apollo 16 photography was performed with a 35-mm Nikon camera with a 55-mm f/1.2 lens and 2485 film. The base fog on the film was 0.54 compared to the base fog of 0.07 on the SO164 film. This high fog is attributed to the higher susceptibility of the 2485 film to radiation damage. See Appendix B for the properties of type 2485 film.

The first sequence was taken with the sun 43 deg below the camera axis. The field of view included sun angles from 25 deg to 61 deg. The camera was then rotated by 30 deg to give sun angles ranging from 55 deg to 91 deg. Moonlight was not directly incident on the window surface but did illuminate the bottom edge of the window seal. Strong reflected glare from this edge may be seen in Figure 3, and some scattered light may be seen above this edge. The large object in the center is planet Venus. Taking the darkest region on the photograph where scattered moonlight is minimized, the background brightness at various sun angles is measured to be $10^{-11.5}$ $B_{\odot}$ at 26 deg to $10^{-12.4}$ $B_{\odot}$ at 76 deg.

The third and fourth sequences were taken with the spacecraft axis at 120 deg to the sun. Again, by moving the camera 30 deg, sun angles from 102 deg to 168 deg could be viewed. Unfortunately, in this orientation, portions of the window were directly illuminated by moonlight (Fig. 4). The brightness of the illuminated portions was

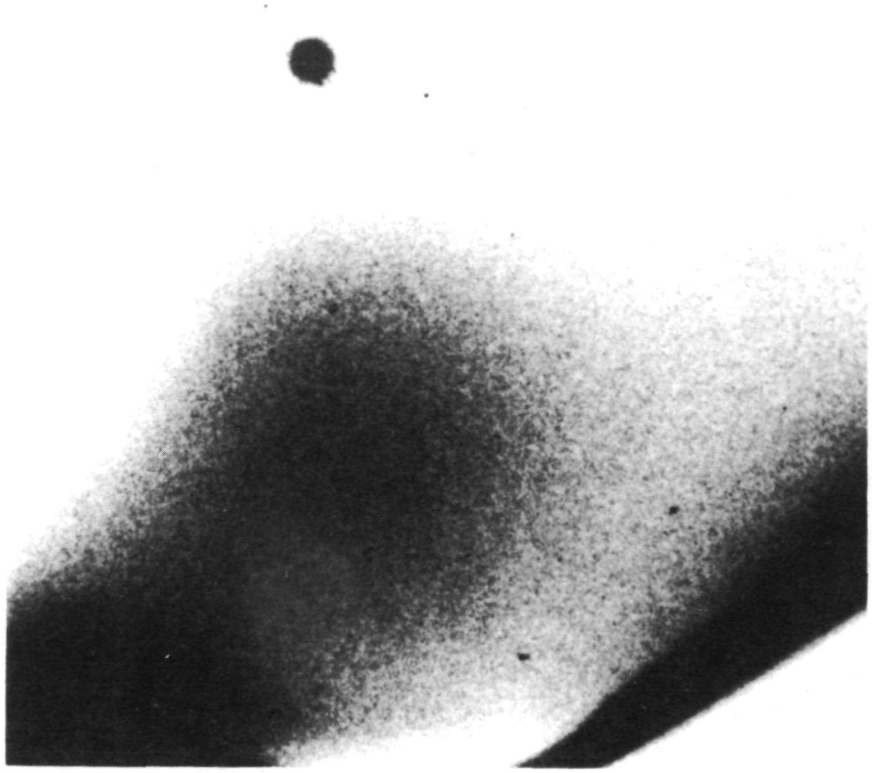

Figure 3. Apollo 16 star-field photograph taken at 1 sec, f/1.2 on 2485 film. Print was reproduced from a second generation positive which also produced right-left reversals. Glare from moonlight scattered from the lower window edge is visible in the lower portion of the frame. The ecliptic runs vertically through the center. The bright object in the center is Venus (m_v = 4.2) flanked by β-Taurus (m_v = 1.65) and Mars (m_v = 1.8). Bright object in the low right is Aldeberan (m_v = 0.86) and bright object at bottom center is Saturn (m_v = 0.4). The sun is 43.7 deg below Venus and 29.7 deg below Saturn. The moon is 106.9 deg above Venus.

Figure 4. Apollo 16 star-field photograph similar to Figure 3. The two objects in the upper right are α and β-Centauri (m_v = 0.01 and 0.63). The group of five stars just above and left of center is α through ϵ-Crucis (m_v = 0.85 to 3.5). The pair of stars near center are α and β-Muscae (m_v = 2.7 and 3.06). The sun is 122 deg from α-Muscae, but the moon is at 80 deg. The dark portion of the frame is scattered light from direct illumination of the window by the moon. The portion where stars are visible was shadowed from direct moonlight.

$10^{-10.24}$ $B_{\odot}$. This corresponds to a scattering fraction of 0.038, which does not seem to be an unreasonable value for a triple-pane window exposed to 270 hours of space environment. Heinisch found scattering fractions ranging from 0.0001 to 0.0005 for freshly cleaned single-pane windows in the lab and values of 0.01 to 0.05 for "dirty" single-pane windows [6]. Using the portions of the window that were shadowed from direct moonlight, the observed brightness was $10^{-12.60}$ $B_{\odot}$ at a sun angle of 168 deg.

During this sequence, the camera axis is nearly in the plane of the ecliptic. The zodiacal background ranges from $10^{-11.93}$ $B_{\odot}$ at 26 deg to $10^{-13.15}$ $B_{\odot}$ at 130 deg. Therefore, a large fraction of the observed background may be natural. Figure 5 shows the resulting brightness as a function of sun angle. The higher values are most likely attributed to scattered moonlight, and the minimum values may be scattered light from spacecraft debris. Using the value $10^{-11.5}$ $B_{\odot}$ at 26 deg and assuming that all particles are of such a size to maximize the diffraction phase function, the upper limit for the obscuration fraction is 2.2×10^{-7}.

It is interesting to note that despite an increase in sensitivity by a factor of approximately 70 over the SO164 film used in the Apollo 15 photography, the plate limit for 2485 film is not any fainter than for SO164. This is because of the larger grain size which reduces the quantum detection efficiency and because of the statistical fluctuations in the high fog background. This fact should be remembered when choosing film for space application.

A liquid dump consisting of approximately 12 kg of water and urine was performed shortly after the Apollo 15 star-field sequence. Additional photographs were taken from 1.30 to 28 minutes after the dump to investigate clearing times.

Photographs of the particles are shown in Figure 6. It is interesting to note that particles still appear to be close to the spacecraft even 28 minutes after the dump, as evidenced by the long out-of-focus tracks. It is also curious to note the curved trajectory in the photograph taken at 25 minutes after the dump. This curvature must be real rather than the result of spacecraft motion because other tracks that begin and end in the field of view appear straight. The only plausible explanation of this curvature appears to be an electrostatic interaction between the particle in question and another particle too small to be seen or not in the field of view.

The brightness of the dump-induced cloud was measured by film photometry. A densitometer with a 4-mm spot corresponding to a 12.8 deg field of view was used to integrate the total brightness, including the particles large enough to be seen as individual tracks. A microdensitometer was used to obtain the background from the smaller unresolved particles that produce a scattering haze around the spacecraft. Figure 7 shows the results of these measurements compared to the predicted brightness decay, assuming the particles leave the spacecraft uniformly during the dump with average velocity of 6 m/sec. It is evident that the observed decay initially behaves as the model predicts, but

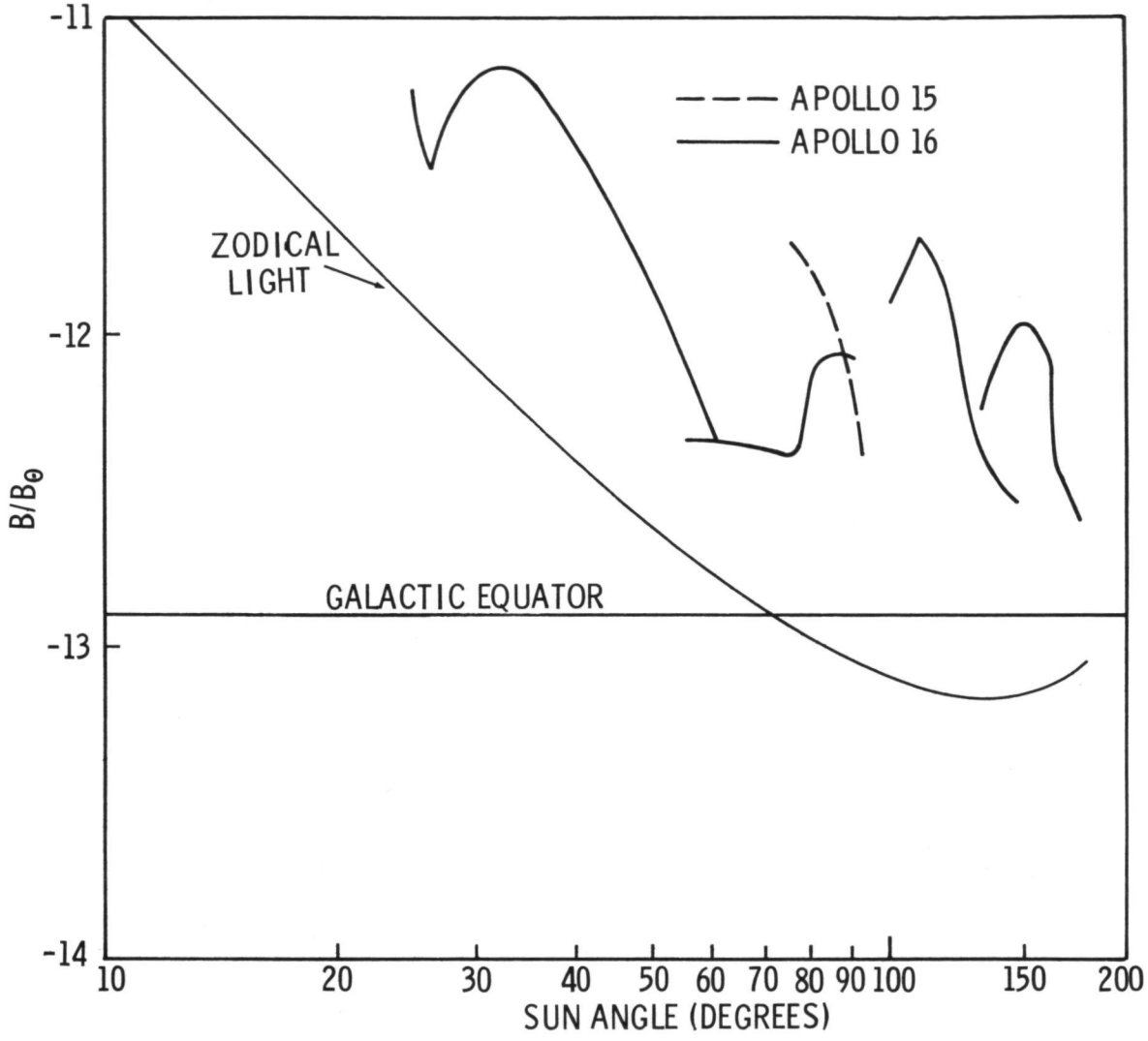

Figure 5. Observed background brightness from Apollo 15 and 16 photography compared with zodiacal light and galactic background. The upper values of observed brightness result from scattered moonlight directly incident on the windows. The lower values are taken from regions not directly exposed to moonlight, but probably have some scattered moonlight or internal light incident on the window.

apparently additional material leaves the spacecraft for many minutes after the dump. This is also consistent with the fact that particles were seen near the spacecraft in the later photographs. This effect is caused by the formation of an ice cone around the nozzle (Fig. 8) and also by the formation, in the nozzle, of a freeze plug that periodically sublimes away, allowing more liquid to be vented.

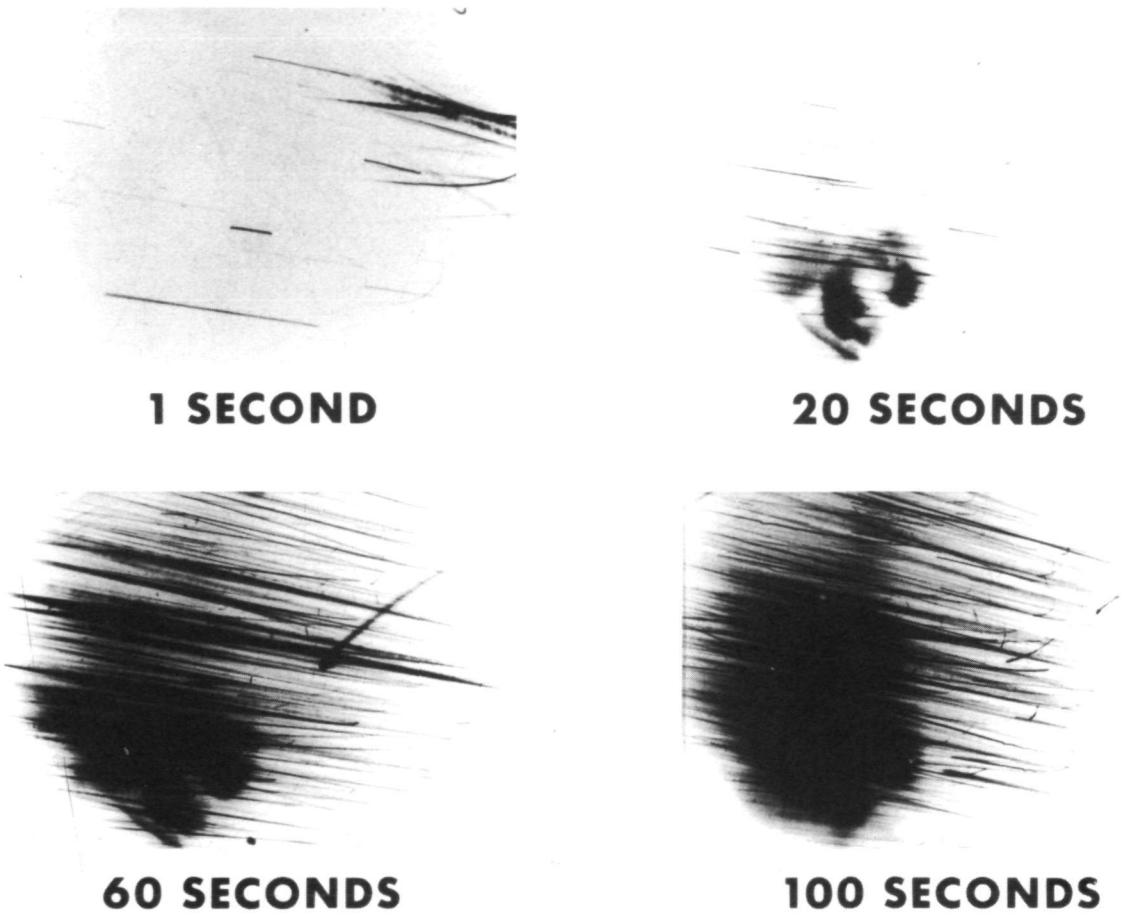

Figure 6. Photographs taken 25 to 28 minutes after liquid waste dump from Apollo 15. Dark spot left of center is the reflected light seen in Fig. 2. Curved tracks seen in the long exposures are the result of slight angular rates of the spacecraft. The broad tracks are out-of-focus nearby particles. However, the curved tracks in the one-second exposure appear to be actual particle trajectories since the spacecraft did not drift during the exposure as evidenced by the straight tracks that begin and end in the field of view.

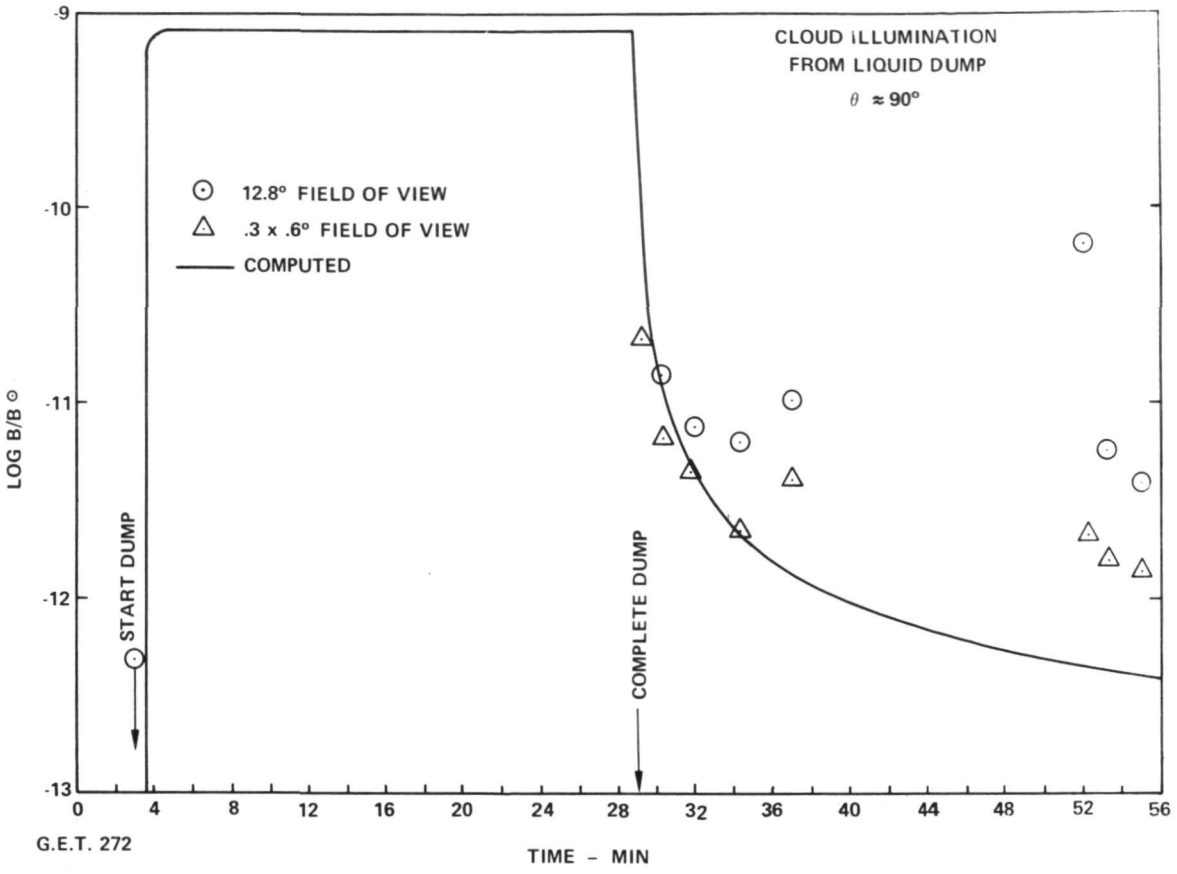

Figure 7. Predicted and observed clearing times for the Apollo water dump. The circles are measured brightness from a 12.8-deg field of view and include the contributions from particles large enough to be seen as individual particle tracks. The triangles are measured brightness from the background of unresolved particles. The predicted brightness assumes the source function terminates at dump completion and that the cloud expands uniformly at 6 m/sec average velocity. The observations initially follow this model, but the fact that material is ejected later is clearly seen.

STELLAR CAMERA

Additional evidence for this continued release of particles comes from the stellar camera on Apollo 15 which photographed navigational stars during lunar mapping sequences. The stellar camera used type 3401 film (Plus-X with an Estar base) which was exposed for 1.5 sec at f/2.8. A background brightness of 10^{-11} $B_{\odot}$ would produce a

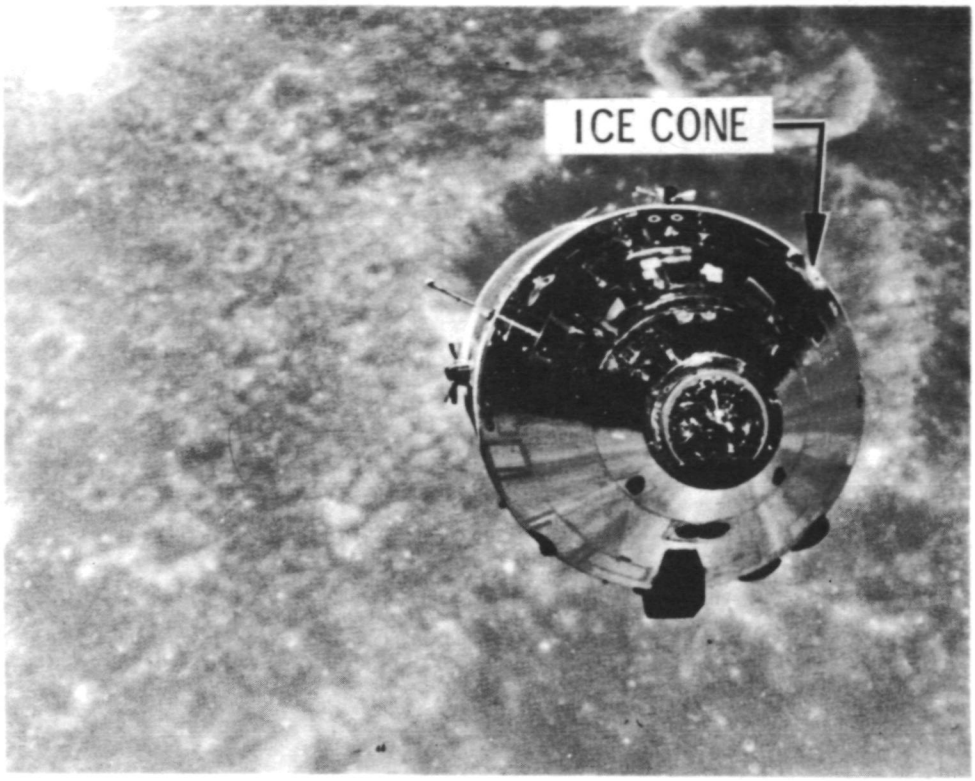

Figure 8. Photograph of an Apollo CM in lunar orbit showing the ice cone formed around the urine dump nozzle.

detectable density change. The minimum density measured was 0.60 to 0.89 on both Apollo 15 and 16, which corresponds to $10^{-10.23}$ to $10^{-10.07}$ $B_{\odot}$. It is quite likely that a large portion of this background can be attributed to moonlight reflected from the Service Module (SM) surface into the glare shield (Appendix C). This camera did on several instances observe many particles near the spacecraft during the first orbit or two after the camera was activated following a liquid dump (Fig. 9). (Usually the camera was inhibited for one or two orbits following a dump). These particles generally appeared not at orbital sunrise but after terminator crossing. Their trajectories appear to converge toward the location of the dump nozzle. These facts indicate that the particles are not co-orbiting with the spacecraft but are frozen to the ice cone in the nozzle region. Apparently the lunar infrared radiation received after terminator crossing is necessary to cause sufficient melting for particle release, although it is also possible that the time required after orbital sunrise for the ice to melt sufficiently to produce particles is approximately the time between orbital sunrise and terminator crossing.

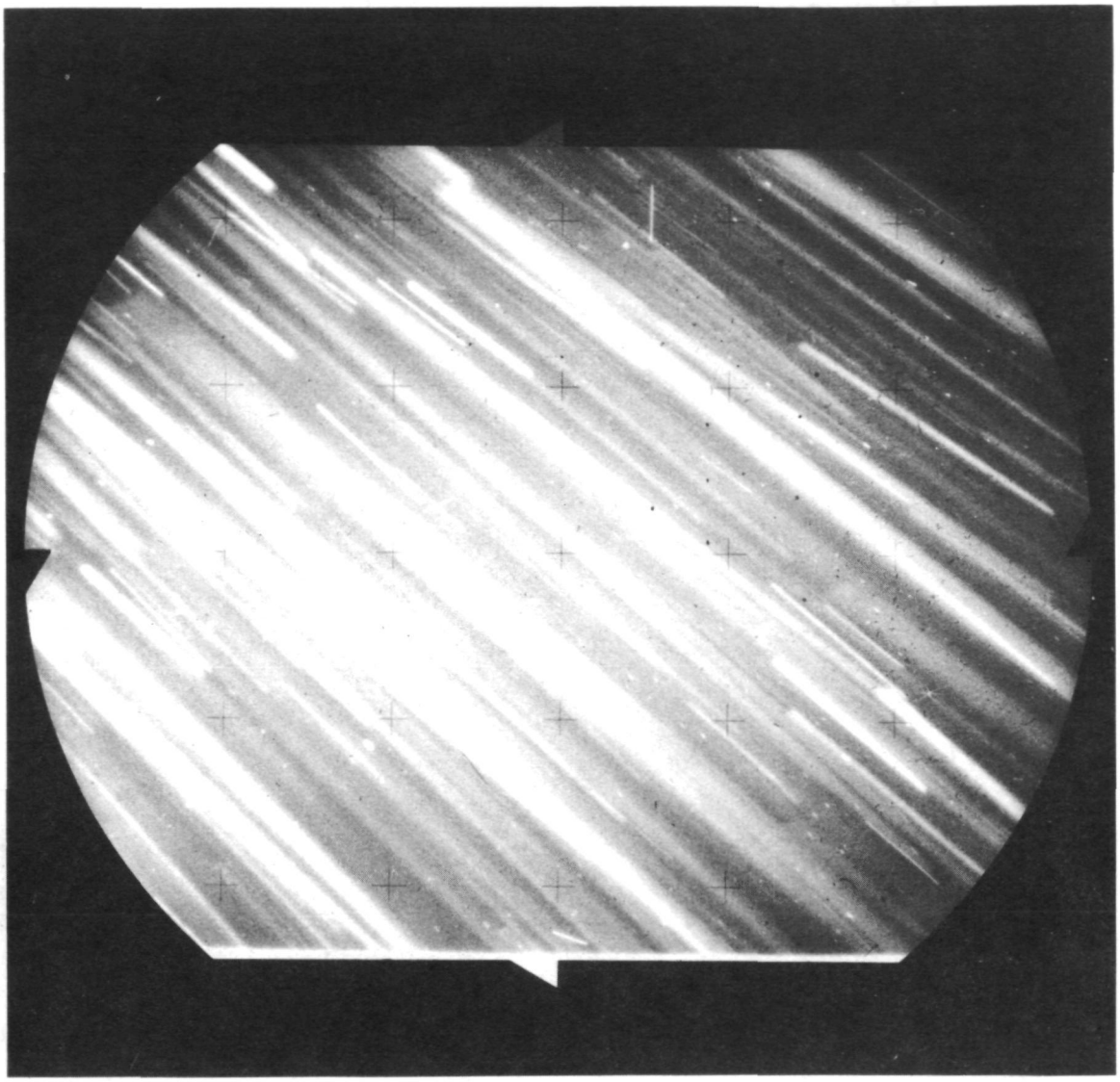

Figure 9. Apollo 15 stellar camera photograph taken at 1.5 sec at f/2.8 on 3401 film. This was just after terminator crossing several orbits after a liquid dump. The particle tracks appear to converge toward the upper left, which is the vicinity of the dump nozzle.

Out of 2338 usable frames from the Apollo 15 stellar camera, 160 showed particle tracks. The field of view was 0.131 steradians. This results in a probability of one or more particles being in the field of view of 0.52/steradian, or 0.35 particles/sec/steradian.

ULTRAVIOLET SPECTROMETER

Apollo 17 carried an ultraviolet spectrophotometer that operated in the region from 117.5 nm (1175 Å) to 167.5 nm (1675 Å) [7]. If there is a significant number of ice crystals in the vicinity of the spacecraft, the instrument could possibly detect reflected or scattered light from them. Since the 121.6 nm (1216 Å) Lyman line is the most intense radiation available, this was monitored as the spacecraft entered the lunar shadow at a sun angle of 160 deg. No change was observed, and the limit of detectable change was estimated to be 1 Rayleigh.

One Rayleigh at 121.6 nm (1216 Å) is equivalent to 1.3×10^{-6} ergs cm^{-2} sec^{-1} sr^{-1}. The solar flux at 121.6 nm (1216 Å) is taken to be 6 ergs/cm^2/sec. The phase function for a sphere is $2A (\sin \theta - \theta \cos \theta)/3\pi^2$, where A is the albedo. The brightness of the reflected light is, therefore,

$$B = N_c \pi a^2 \frac{2A}{3\pi^2} (\sin \theta - \theta \cos \theta)\, 6 \frac{\text{ergs}}{\text{cm}^2 \text{ sec}} \leqslant 1.3 \times 10^{-6} \frac{\text{ergs}}{\text{cm}^2 \text{ sec sr}} , \qquad (1)$$

where

$$N_c \pi a^2 \leqslant \frac{1.08 \times 10^{-6}}{A} \qquad (2)$$

Taking the albedo of the ice crystals at Lyman alpha to be 0.04, the upper limit for the obscuration fraction, $N_c \pi a^2$, is 2.7×10^{-5}. If the number of ice crystals was actually large enough to produce this obscuration fraction, the visible scattered light background would be 10^{-10} $B_\odot$ at a 90-deg sun angle.

The spectrometer is capable of detecting a column density of $10^7/cm^2$ atomic hydrogen. Assuming a disassociation time of 10^6 sec, a column density of 10^{13} H_2O molecules per cm^2 should be detectable. No evidence of such column density was observed except during a liquid dump. Even in this case, the signal decayed very rapidly after the event, signifying the rapid dispersal of dump products.

During the course of the mission, the spectrometer response was observed to degrade by approximately 17 percent. This was attributed to aging of the electron multiplier and is an expected degradation for the total photon flux counted by the instrument. A Reaction Control System (RCS) plume was fired directly over the

instrument toward the latter phase of the mission. The spectrometer responded to the light in the plume but showed no degradation that could be attributed to the RCS material depositing on the optics. However, the entrance to the instrument is a 2 mm by 57 mm slit that is well baffled from stray light. The plume was directed over the top of the instrument and not directly into the aperture, but it can be said that even very sensitive far-ultraviolet instruments can be operated in the vicinity of RCS engines if reasonable care is taken.

MASS SPECTROMETER

Additional contamination data were obtained from the Apollo 15 and 16 mass spectrometer [8]. This instrument was mounted on a 6.1-m (20-ft) boom to avoid influence from the spacecraft and had an entrance hood with an entrance aperture that would accept a 2π steradian solid angle. The hood was oriented such that the spacecraft was excluded from the field of view. No molecule leaving the spacecraft could enter the aperture by traveling a straight line. The purpose of the instrument was to analyze lunar atmosphere by orienting the spacecraft such that the aperture was directed along the velocity vector. The instrument was also flown such that the aperture looked opposite to the velocity vector to see how much molecular flux was attributable to spacecraft background.

When the instrument was activated in lunar orbit, the maximum observed flux was approximately 4×10^{12} molecules/cm^2/sec H_2O and 10^{11} molecules/cm^2/sec CO_2. There were peaks at each mass number indicating hydrocarbons, but these peaks were orders of magnitude lower than the H_2O and CO_2 peaks. The observed flux reached its maximum value at orbital noon and dropped by a factor of 4 or 5 on the dark side.

Surprisingly, the situation was almost identical when the spacecraft was turned around so that the entrance aperture was opposite the velocity vector. Since lunar orbital velocity is approximately 1.5 km/sec and average molecular velocities in the lunar atmosphere are 500 m/sec, very few atmospheric molecules could enter the detector when it was opposite to the velocity vector. Therefore, it is obvious that the fluxes observed by the mass spectrometer must be associated with the spacecraft. It is difficult to understand how molecules leaving the spacecraft with velocities of hundreds of m/sec could possibly return. Certainly scattering between the outgoing molecules would be too small to produce the observed fluxes. The maximum column density of 10^{13} molecules/cm^2 imposed by the Apollo 17 ultraviolet spectrometer implies an upper limit of 6.8×10^{14} molecules/cm^2/sec leaving the spacecraft. Since all molecules that leave have a net radial velocity, collisions that could result in a negative radial velocity are extremely rare. Even neglecting this fact and assuming that collisions are isotropic relative to the spacecraft, an upper limit can be placed on the backscatter which is several orders of magnitude below the observed flux. The lunar atmosphere is insufficient to cause this much scattering; and even if this were the return mechanism, the backscattered molecules would only be seen when looking into the velocity vector.

The Apollo 16 mass spectrometer had an additional provision to allow the entrance hood to be baked out in orbit to remove any possible contaminants. Despite this precaution, it performed almost the same as the one on Apollo 15. It is possible that the observed molecules could originate within the analyzer section of the instrument where most of the electronics are located. Such molecules could find their way out of the entrance slit, become ionized by the ionizer, and then be analyzed. No doubt, some of the background results from this. However, this does not explain the fact that a strong diurnal effect is seen and that the peak readings which are 4 to 5 times the background coincide with orbital noon. Temperatures inside the instrument which would govern the internal outgassing rate would be expected to peak near orbital sunset, not orbital noon.

As the spacecraft left the moon, the observed flux diminished. The liquid dump photographed during the Apollo 15 trans-earth-coast produced only a very slight increase in the observed H_2O flux. This demonstrates that the molecular species resulting from the dump travel in straight lines and do not get scattered back toward the spacecraft. The observed flux is most likely sublimation products from the ice crystals that pass into the field of view of the mass spectrometer. Since ice crystals have a very low absorptivity for visible light, they melt very slowly unless they receive long wavelength infrared radiation from a nearby planet. This would account for the fact that the observed flux was so much lower, even when large quantities of H_2O were being dumped, during trans-earth-coast than in lunar orbit.

ANALYSIS

It was first thought that the mass spectrometer was reencountering molecules that had left the spacecraft and were spread along the orbital path. A simple calculation shows, however, that even molecules leaving a cold surface such as a subliming ice crystal would have average velocities of nearly 500 m/sec. Their trajectories would deviate as much as several hundred kilometers from the spacecraft's path. To populate such a volume to the density required to give the observed flux, approximately 9 million kg (10,000 tons) of H_2O would have to be released.

It has been suggested that a charge interaction might tend to contain a cloud of molecules in the vicinity of a spacecraft. This does seem reasonable because of the following considerations. First, even in cislunar space the solar plasma can provide currents as high as 10^{-7} amps/m^2, which can discharge a 2-m radius sphere at the rate of 20,000 volts/sec [9]. Therefore, spacecraft potentials are not generally more than a few volts. The escape velocity for an H_2O ion at the surface of a 2-m radius sphere at 1 volt is $\sim$ 3000 m/sec. If neutrals become ionized at some distance r, the escape velocity diminishes by $r^{-1/2}$. At approximately 100 m the escape velocity is comparable to molecular speed if Debye shielding is ignored. For a Debye length of 10 m, which is typical of cislunar space, the escape velocity drops to molecular speed at 16 m. Typical

ionization times are 4×10^6 sec. Therefore, the probability of a molecule returning as an ion is 5.3×10^{-8} for an infinite Debye length and 8.5×10^{-9} for a Debye length of 10 m. Since the outgoing flux can be no more than 6.8×10^{14} molecules/cm^2/sec, the return flux of ions is limited to 3.6×10^7 molecules/cm^2/sec with no Debye shielding and 5.8×10^6 molecules/cm^2/sec for a Debye length of 10 m. Therefore, this mechanism falls short by 5 to 6 orders of magnitude. The potential required to produce the observed return flux would be 110 kV, ignoring Debye shielding, and would be virtually infinite for a 10-m Debye length.

Since H_2O molecules have a dipole moment of 6×10^{-30} Coulomb, they will interact with a field gradient and be attracted toward the spacecraft. However, for a 2-m radius sphere at 1 volt potential, the escape velocity is only 0.014 m/sec. For molecules leaving the surface with a Maxwell-Boltzmann distribution, the fraction that would have less than this velocity is only 1.4×10^{-14}. Therefore, the return flux would be ~ 1 molecule/cm^2/sec. To produce the observed return flux by this interaction, the escape velocity would have to be 104 m/sec. This would require a potential of 53 million volts, neglecting Debye shielding.

The only conceivable mechanism that could produce the observed return flux requires a cloud of sublimating ice crystals in the vicinity of the spacecraft. The flux from sublimating particles can be estimated in the following manner. Let the detector have a field of view ω. The number of ice crystals in the field between r and r + dr is $N(r)\, r^2\, dr\, d\omega$, where N(r) is the number density of the ice crystals. Each crystal emits molecules at the rate $\dot{m}$ per unit area multiplied by $4\pi a^2$, where a is the radius. The molecular flux reaching the detector per unit time is $4\pi a^2\, \dot{m}\, d\Omega/4\pi$, where $d\Omega$ is the solid angle subtended by the detector, which is given by the projected detector area divided by r^2. Therefore, the observed molecular flux for an isotropic distribution and a 2π steradian field of view is

$$\phi_{obs} = \int_{R_0}^{R_m} dr \int_0^{\pi/2} 2\pi \sin\theta\, N(r)\, r^2\, 4\pi a^2\, \frac{\dot{m} \cos\theta}{4\pi r^2}\, d\theta \quad , \tag{3}$$

where R_0 is the distance from the origin (r = 0) to the viewing point and R_m is the distance traveled before the particle melts.

Integrating over θ yields

$$\phi_{obs} = \dot{m} \int_{R_0}^{R_m} N(r)\, \pi\, a^2\, dr \tag{4}$$

If the particles are melting, a is a function of time. Since $\dot{m}$ is the evaporation rate per unit area, $\dot{a} = \dot{m}/\rho$, where ρ is the density. If the evaporation rate is constant in time, $a = a_0 - at$. If the particles move with radial velocity v, $a = a_0(1 - r/R_1 + R_0/R_1)$, where $R_1 = a_0 v \rho/\dot{m}$ and is the distance the ice crystal travels before it melts.

The number density N(r) can be estimated by considering the particle cloud to be expanding isotropically with radial velocity v. Therefore,

$$\dot{N}(r) = \frac{\dot{N}_T}{4 \pi r^2 v} \quad , \tag{5}$$

where $\dot{N}_T$ is the source rate, the number of particles generated per unit time. Representing the particles as spheres with radius a_0,

$$\dot{N}_T = \frac{3 \dot{M}_T}{4 \pi a_0^3 \rho} \quad , \tag{6}$$

where $\dot{M}_T$ is the total mass of particles released per unit time.

Inserting these expressions into equation (4) and integrating,

$$\phi_{obs} = \frac{3 \dot{M}_T}{16 \pi R_1^2} \left[\frac{R_1}{R_0} - 2 \left(1 + \frac{R_0}{R_1} \right) \ln \left(1 + \frac{R_1}{R_0} \right) + 2 \right] . \tag{7}$$

To calculate the evaporation rate, it is first necessary to obtain the temperature of the ice crystals. This is done by balancing the heat input against the heat lost to radiation, plus the heat loss to sublimation. Assuming the ice crystals have an albedo of 0.9, which is typical for snow, the energy input from the sun only will result in a temperature of 158°K, which yields $\dot{m}$ of 6.98×10^{-9} gm/cm^2/sec. If the average infrared radiation from the moon is added, the temperature of the ice crystal goes to 185°C, yielding an evaporation rate of 1.86×10^{-6} gm/cm^2/sec. Over the subsolar point, where surface temperatures are nearly 400°K, an ice crystal would go to 195°K and evaporate at 9.97×10^{-6} gm/cm^2/sec.

For ϕ_{obs} = 1.2 x 10^{-10} gm/cm^2/sec (4 x 10^{12} H_2O molecules/cm^2/sec) and R_0 = 200 cm, the mass emission rate required to give the observed return flux is shown in Figure 10 as a function of R_1. Also shown is the rate at which material could be released without violating the column density limit. It may be readily seen that the

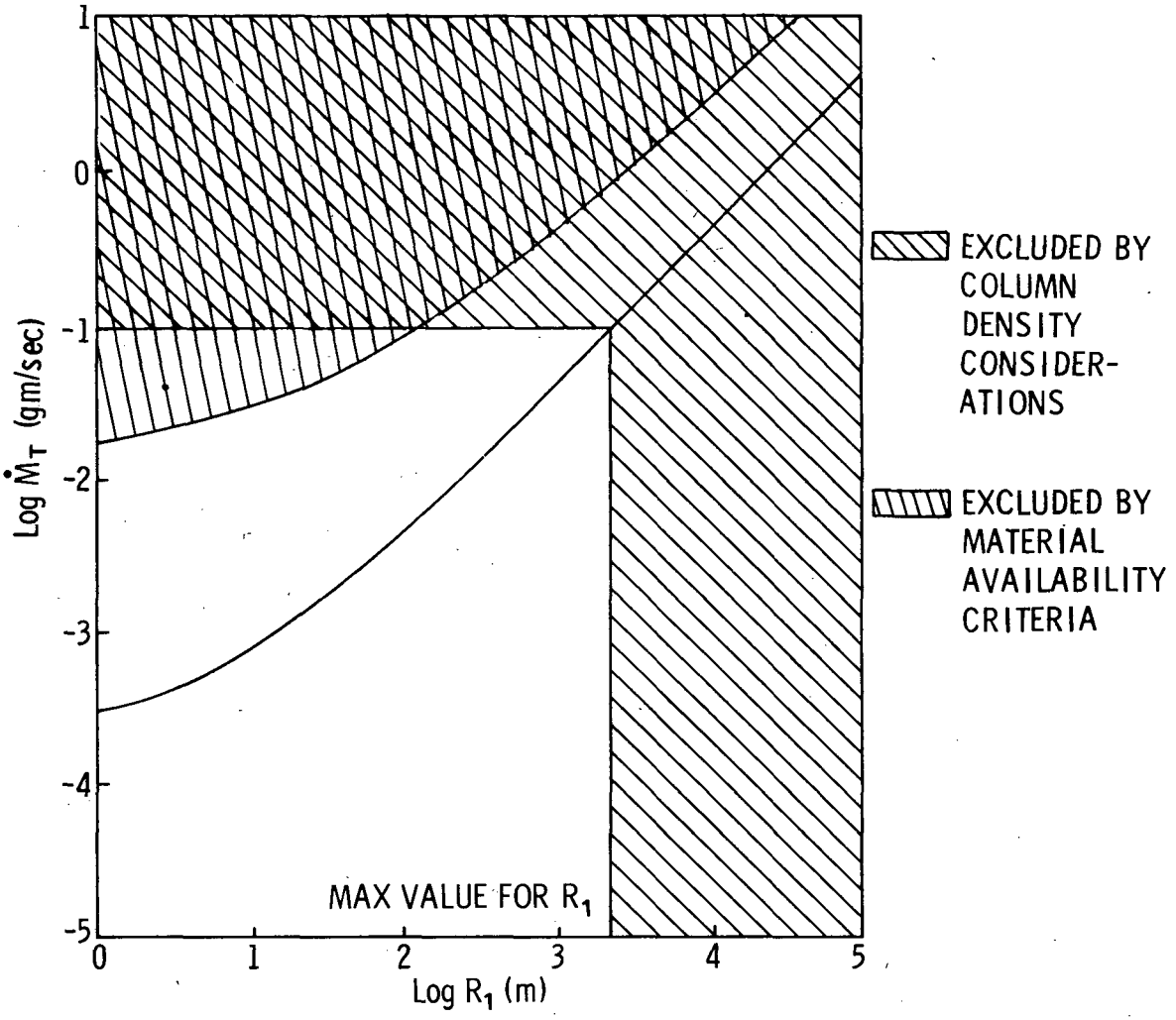

Figure 10. Average rate of material loss in the form of ice crystals to account for observed return flux as a function of distance particles travel before melting. A value of 0.093 gm/sec is taken as the maximum rate of material loss that can reasonably be sustained from the amount of ice available. This sets an upper limit of 2100 m on the distance traveled before melting. The upper curve indicates the rate of loss that would produce greater than 10^{13} molecules/cm^2 column density.

amount of released material required to produce the observed return flux is always less than the maximum allowable release set by column density considerations. However, if it is assumed that 10 percent of the 20 kg of H_2O dumped overboard freezes in the vicinity of the nozzle and flakes off at an average rate one-fourth that required to produce the peak return flux, the maximum rate cannot be greater than 0.093 gm/sec, and this sets a limit for R_1 of 2100 m.

A second constraint to be considered on the amount and size of material released is the scattered light background and the visibility of the particles. The total scattered light background is given by

$$\frac{B}{B_\odot} = \omega_\odot \int_{R_0}^{R_m} N(r) \left(\frac{d\sigma}{d\Omega}\right)_\theta dr \quad , \tag{8}$$

where $B_\odot$ and $\omega_\odot$ are the brightness and solid angle of the sun, respectively.

For particles such that $a >> \lambda$ and for sun angles $\theta \geqslant \pi/2$, the scattering cross section is predominantly reflection. Considering the ice crystals as Lambertian spheres,

$$\left(\frac{d\sigma}{d\Omega}\right)_\theta = \pi a^2 \frac{2A}{3\pi^2} (\text{si}\ \theta - \theta \cos\theta) \tag{9}$$

where A is the albedo.

Note that the integral now has the same form as the expression for ϕ_{obs}. In fact, the brightness and return flux are related by

$$\frac{B}{B_\odot} = \omega_\odot \frac{2A}{3\pi^2} (\sin\theta - \theta\cos\theta) \frac{\phi_{obs}}{\dot{m}} \tag{10}$$

For $\theta = \pi/2$, A = 1, and $\dot{m} = 10^{-5}$ gm/cm^2/sec, a return flux of 1.2×10^{-10} gm/cm^2/sec would necessarily require a background brightness of $10^{-10.3}$ $B_\odot$. This is just below the 10^{-10} $B_\odot$ detectable upper limit set by the ultraviolet spectrometer and is the same order of magnitude of brightness observed on the stellar camera. Unfortunately, however, since reflection from the lunar surface off the spacecraft structure into the glare shield would be expected to produce the same order of magnitude effect, the fact that a scattering background of this magnitude was observed by the stellar camera does not confirm or rule out the existence of the particle cloud.

Something can be said concerning the size distribution of the particles from the fact that the stellar camera detected only 0.52 particles/steradian per frame. If particles are being produced at the rate of $\dot{N}_T$ and leave the spacecraft isotropically, the number entering the field of view is $\dot{N}_T/4\pi$ particles/sr/sec. If the exposure time is t_e, the total number of particles seen will be those produced during this time, $\dot{N}_T t_e/4\pi$, plus those already in the field of view when viewing commenced. This number is $\dot{N}_T (R_{max} - R_{min})/4\pi v$, where R_{max} is the greatest distance a particle could be seen and R_{min} is the closest distance a particle could be seen. Therefore,

$$N_{obs} = \frac{\dot{N}_T}{4\pi}\left(t_e + \frac{R_{max} - R_{min}}{v}\right) \tag{11}$$

Since the film was fogged to a density of 0.8, it is difficult to detect any but the brightest stars. If it is assumed that a density of 3.0 is required to detect an image, the exposure necessary is 0.59 meter-candle-sec. A stationary point source produces an exposure given by

$$E_f = \frac{\pi d_L^2 I_p t_e}{4 A_{film}} \tag{12}$$

where d_L is the diameter of the objective lens, t_e is the exposure time, and A_{film} is the area covered by the image on the film. The intensity I_p of a Lambertian sphere with a radius a at distance R and at a 90-deg sun angle is

$$I_p = \frac{2\pi a^2 I_\odot}{3\pi^2 R^2} \tag{13}$$

where $I_\odot = 1.365 \times 10^5$ lumens/m^2. Therefore,

$$E_f = \frac{d_L^2 t_e I_\odot a^2}{6 A_{film} R^2} \tag{14}$$

The stellar camera was equipped with a 76-mm, f/2.8 lens. Therefore, d = 0.027 m. Star images from the Apollo 15 photography covered areas of approximately 1000 mm^2 or 10^{-9} m^2. This represents the point spread function (PSF) of the lens plus the spacecraft jitter and will be taken as a typical value for A_{film}. With these values, a minimum detectable object must be brighter than $m_v = 1.46$, which is consistent with the fact that only the brightest stars were apparent.

A nearby particle at distance R will appear out of focus and will produce an image whose size is

$$d_f = \frac{F\, d_L}{R} \tag{15}$$

where F is the focal length. If the particle is moving with a perpendicular component $v_\perp$, the writing speed will be $v_\perp$ F/R. The image, therefore, sweeps out an area at the rate

$$\dot{A} = \frac{v_\perp \cdot F\, d_f}{R^2} = \frac{v_\perp\, F^2\, d_L}{R} \tag{16}$$

The exposure is given by

$$E_f = \frac{\pi}{4} \frac{d_L{}^2 \cdot I_p}{\dot{A}_{film}} = \frac{d_L\, I_\odot\, a^2}{6\, v_\perp\, F^2} \tag{17}$$

The perpendicular component of v from a particle leaving from a point whose perpendicular distance from the line of sight is $R_\perp$ is given by

$$v_\perp = \frac{v\, R_\perp}{\left(R^2 + R_\perp{}^2\right)^{1/2}} \tag{18}$$

Note that the exposure produced by a nearby moving particle increases with R because the writing speed is reduced. Therefore, the minimum range at which a particle can be seen is

$$R_{min} = R_{\perp}\left[\left(\frac{6\, v\, F^2\, E_f}{d_L\, I_{\odot}\, a^2}\right)^2 - 1\right]^{1/2} \tag{19}$$

Eventually, the image size is limited by the PSF and spacecraft jitter. The maximum range at which a particle may be seen is given by the visibility criteria for stationary particles, equation (14),

$$R_{max} = \left(\frac{d_L^2\, t_e\, I_{\odot}\, a^2}{6\, A_{film}\, E_f}\right)^{1/2} \tag{20}$$

Figure 11 is a plot of the number of particles per steradian that would be seen by the stellar camera as a function of a_0 and v in order to account for the return flux observed by the mass spectrometer. Of course, no particles will be seen if $R_{max} < R_{min}$. If $R_{max} \geq R_{min}$, the number increases very abruptly to a number more than 3 orders of magnitude higher than what was observed. To stay below the constraint set by the fact that very few bright particles were seen in the vicinity of the spacecraft, either $R_{max} < R_{min}$ or a_0 must be greater than several hundered centimeters. The latter is not possible because the mass outflow required if the return flux is to be produced by large chunks of ice far exceeds the amount available. The fact that few or no particles were seen, therefore, requires $R_{max} < R_{min}$. Equating equations (19) and (20) and taking advantage of the fact that $6\, v\, F^2\, E_f / d_L I_{\odot} a^2 \gg 1$, a relation between a and v may be found; i.e.,

$$a^3 = \frac{6^{3/2}\, F^2\, E_f^{3/2}\, A_{film}^{1/2}\, R_{\perp}\, v}{d_L^2\, I_{\odot}^{3/2}\, t_e^{1/2}} \tag{21}$$

Actually, the a's in equations (19) and (20) are a function of distance; however, the point of intersection between R_{max} and R_{min} is at a distance $\ll R_1$. Therefore, the effect of melting can be neglected except for very small velocities (Appendix D).

The various constraints on the size and velocity distribution are shown in Figure 12. In addition to the material availability criterion discussed previously, which sets an upper limit of $R_1 = \rho a v / \dot{m}$, and the visibility criterion above, there is another constraint, a minimum size for R_1. If the melting distance R_1 is not greater than the distance from

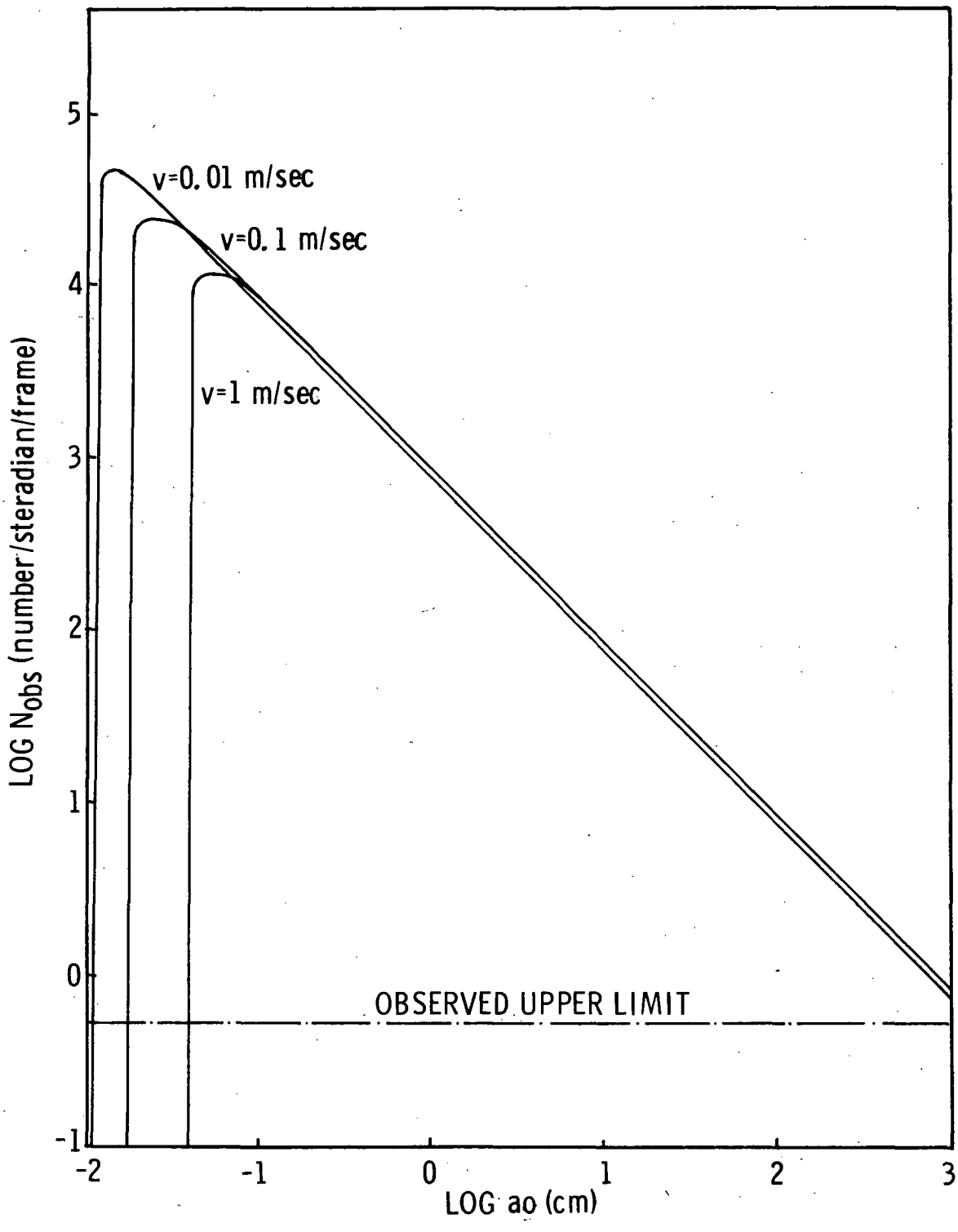

Figure 11. This indicates the number of individual ice particles that would be readily discernable on the Apollo 15 stellar camera as a function of their initial radius, assuming the observed return flux was attributed to sublimation of these particles. This sets an upper limit on the size of particles generated.

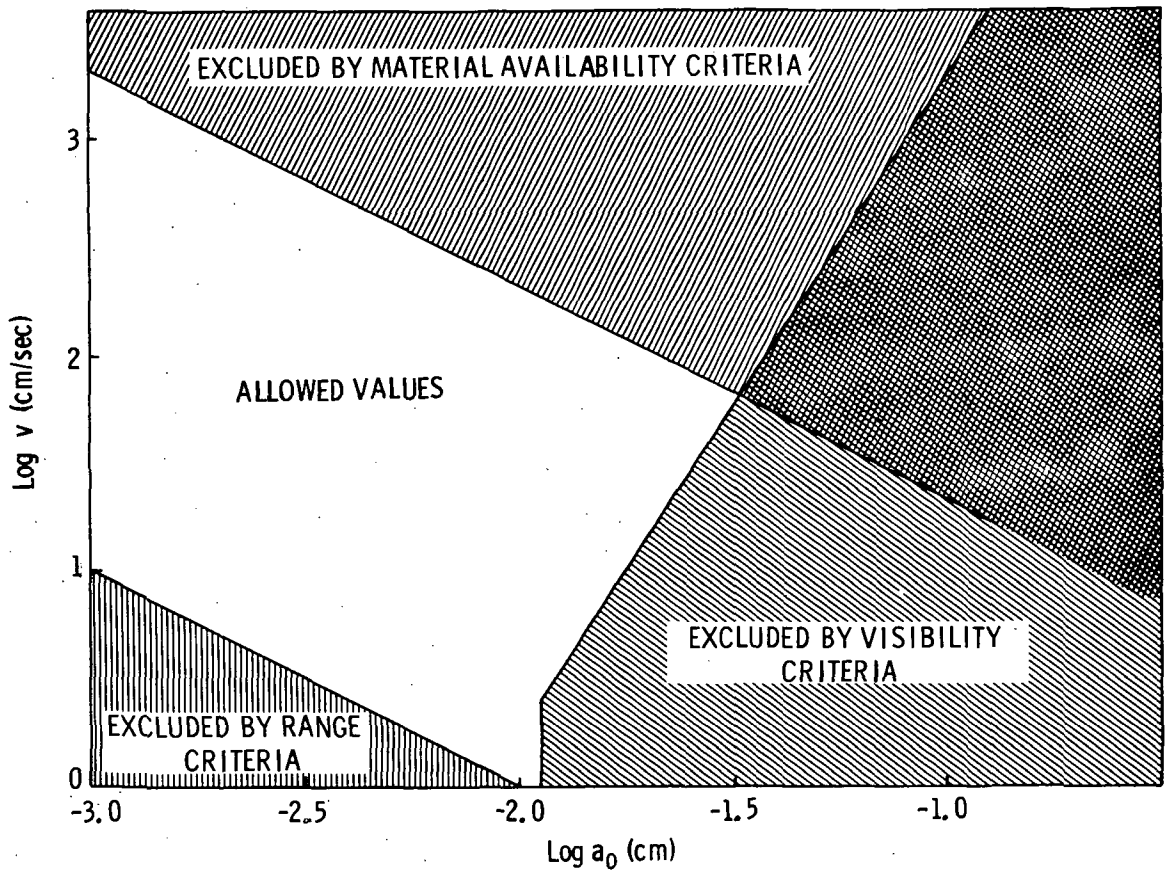

Figure 12. Constraints on particle size and velocity placed by the various observations on Apollo 15 and 16. Particles responsible for the observed return flux must lie in the allowed region. Particles smaller than 111 micron radius will melt before they move out far enough to become visible, regardless of their velocity. However, unless their velocity is larger than a few cm/sec they will melt before they move beyond the mass spectrometer and, therefore, will not contribute to the observed flux.

the source to the mass spectrometer, no return can be observed. Taking an arbitrary value of 10 m as the minimum distance the particles traverse before they completely melt (if the distance were much less than this, the particles could never get in front of the mass spectrometer), the lower left-hand corner is excluded by $\rho av/\dot{m} \leqslant 10$ m. It may be seen that the particle radius must be less than $\sim 300\ \mu$m and the velocities must range from 0.1 to 10 m/sec if all the constraints are to be satisfied.

DISCUSSION

The unexpected high flux of H_2O molecules observed by the Apollo 15 and 16 mass spectrometer suggests the presence of a cloud of ice crystals in the vicinity of the spacecraft. These ice crystals must have an average size under ~ 100 μm or they would appear as bright stars in all of the stellar camera photographs. If they are to evaporate fast enough to account for the flux observed by the mass spectrometer, their lifetimes must be less than 1 hr. The interval between liquid dumps was much longer than this, and the flux was observed throughout the lunar orbit portion of the mission; therefore, the particles making up the ice cloud must be generated more or less continuously. The obscuration fraction (the integral in equation (4)) is given by the observed flux divided by the evaporation rate per unit area and is 1.2×10^{-5} in lunar orbit. Photographic results during trans-earth-coast indicate an obscuration factor of no more than 2.2×10^{-7}. Obviously, something is different about lunar orbit.

This difference and the fact that the observed flux diminished rapidly as the spacecraft left the moon suggested that some sort of accumulation effect was acting in lunar orbit. However, it has already been demonstrated that molecular accumulation in lunar orbit would require impossible amounts of material in order to become significant. Orbital dynamics will confine ice crystals released by a spacecraft to oscillate about the orbital path with an amplitude given approximately by $r_\odot v/v_\odot$, where $r_\odot$ is the radius vector of the spacecraft, $v_\odot$ is the spacecraft velocity and v is the release velocity. In the absence of drag, the particles will drift away along the orbit with an average velocity given by

$$\dot{S} = \frac{3}{2} v_\odot \left[2 \frac{v}{v_\odot} \cos \gamma + \left(\frac{v}{v_\odot} \right)^2 \right] \tag{23}$$

where γ is the angle between the ejection velocity vector and the orbital path. Since the mass spectrometer looks along the orbital path, it was thought that orbital dynamics, which causes the particles to be concentrated along the orbital path instead of allowing them to expand freely, might account for the much higher column density needed to raise the obscuration factor by 50 in lunar orbit. It can be shown [10] that the ratio of the column density along the orbital path from orbital dynamics to the case for free expansion for particles released isotropically is

$$\frac{n_{c(\text{orbital})}}{n_{c(\text{free})}} = \frac{2^{3/2}}{3} \frac{R_0}{r_\odot (v/v_\odot)^{3/2}} \ln \left(\frac{2 + v/v_\odot}{v/v_\odot} \right) \tag{24}$$

For $r_\odot = 1.6 \times 10^8$ cm, $R_0 = 200$ cm, $v_\odot = 1.63 \times 10^5$ cm/sec, the ejection velocity must be less than 6 cm/sec to produce the orbital accumulation required. With this velocity the particles must be less than 73 microns in diameter in order not to violate the visibility criteria, and they would have an average lifetime of only 33 minutes, and lifetime of only 6 minutes near orbital noon. Since it takes approximately half an orbit for the orbital dynamical effects to concentrate the particles along the orbit, these lifetimes do not seem long enough to allow such effects to become significant.

A more likely explanation is that the ice crystals are generated at a different rate in lunar orbit than during trans-earth-coast, possibly because of the influence of the lunar infrared radiation melting the ice cone that accumulates around the dump nozzles. It is known from the stellar camera photographs that particles large enough to be seen emanate from the nozzles at terminator crossing for several revolutions after a dump. It is not too unreasonable to expect smaller particles to flake off in the same manner throughout the interval between dumps. The Apollo 15 and 16 trans-earth-coast photographs were taken with the dump nozzles shadowed from the sun. In the absence of solar and infrared radiation, the process responsible for small particle generation was probably not operable.

Photographs taken during Apollo 15 trans-earth-coast do not show any individual particles. Sixth magnitude stars were visible, and the limiting exposure required for a point object to be detected was estimated to be 0.112 meter-candle-sec. Using equation (21), the minimum particle that could escape detection is given by

$$a\,(m) \leq 3.82 \times 10^{-5}\, v^{1/3}\ (m/sec) \tag{25}$$

From equations (5) and (6), the obscuration factor for constant a_0 is

$$\int_{R_0}^{\infty} N(r)\, \pi\, a_0^2\, dr = \frac{3\, \dot{M}_T}{16\, \pi\, R_0\, a_0\, \rho\, v} \tag{26}$$

For the max value of 2.2×10^{-7} for the obscuration factor obtained from the trans-earth photographs, the upper limits on particle size and emission rate are shown in Table 1.

TABLE 1. UPPER LIMITS FOR PARTICLE RADIUS AND TOTAL MASS LOSS DURING TRANS-EARTH-COAST

v (m/sec)	a_0 (μm)	$\dot{M}_T$ (gm/sec)
0.01	$\leqslant$ 8.24	$\leqslant 6.07 \times 10^{-7}$
0.1	$\leqslant$ 17.75	$\leqslant 1.31 \times 10^{-5}$
1	$\leqslant$ 38.25	$\leqslant 2.81 \times 10^{-4}$
10	$\leqslant$ 82.40	$\leqslant 6.07 \times 10^{-3}$

CONCLUSIONS

The scattered light from the induced environment of the Apollo Command/Service Module during trans-earth-coast has been determined to be no more than 2 to 2.5 times the zodiacal light background. A substantial portion of the measured background may well be due to moonlight scattered from the window openings. In any event, the measured scatter for sun angles greater than 55 deg is less than the 5.5×10^{-13} $B_\odot$ (20 magnitude/sec^2) specified by the Astronomy Working Group for Space Shuttle Payload Planning [11]. The fact that numerous particles are not apparent in the star-field photographs indicates that particles leaving the spacecraft must have an average size of less than 165 μm, provided their velocity is greater than 10 m/sec. If the velocity is less, the average size limit is reduced. The upper limit on total mass of particles generated, set by the brightness measurements and the size limitations, is 6 μg/sec for velocities greater than 10 m/sec, and substantially less if the velocities are smaller.

The high return flux of H_2O and CO_2 observed in lunar orbit is most probably sublimation of ice crystals in the vicinity of the spacecraft. The ice crystals must be generated more or less continuously and probably come from the ice cone that forms around the H_2O and urine dump nozzles. Urine contains several hundred ppm CO_2 which can explain the presence of this peak in the mass spectra. The constraints placed on the particles by the stellar camera observations limit their average size to less than 100 μm and their velocities to between 0.1 and 10 m/sec. The average mass converted into particles must be from 0.75 to 90 μg/sec, depending on particle size and velocity. The maximum lifetime of the particles before melting is less than 1 hour. The maximum column density for H_2O molecules is estimated to be less than 10^{13} molecules/cm^2 based on the Apollo 17 ultraviolet spectrometer.

George C. Marshall Space Flight Center
National Aeronautics and Space Administration
Huntsville, Alabama, June 1974

APPENDIX A

Calculation of the Average Particle Size From Ground Observations of Liquid Dumps

During Apollo 12 a liquid dump was photographed at 110,000 km. The amount of H_2O released was 12.07 kg (26.6 lb), and the peak integrated brightness was estimated to be $m_v = 12$. A similar dump was observed on Apollo 13 at 67,000 km in which 10.6 kg (23.4 lb) of H_2O were dumped. The estimated brightness was $m_v = 9$.

The intensity of an object illuminated by the sun is

$$I = \frac{I_\odot}{r^2} \left(\frac{d\sigma}{d\Omega}\right)_\theta , \tag{A-1}$$

where:

$I_\odot$ is the solar intensity,

r is the range, and

$(d\sigma/d\Omega)_\theta$ is the differential cross section at a sun angle of θ.

Assuming the ice forms Lambertian spheres with radius a and albedo of 1, the differential cross section at 180 deg sun angle is $(d\sigma/d\Omega)_\theta = 2a^2/3$. The total cross section for the cloud, assuming it is optically thin, is $2\,Na^2/3$, where N is the number of particles in the cloud. This number is obtained by dividing the total mass of ice by the average particle mass. The total mass of ice is taken to be 0.75 of the H_2O dumped overboard. Fifteen percent of the H_2O must evaporate to freeze the remainder, and the other 10 percent is assumed to remain in the snow cone.

The ratio of intensities is related to visual magnitude by

$$\frac{I}{I_\odot} = 10^{0.4\,(m_\odot - m_v)} \tag{A-2}$$

From (A-1) and the above discussion,

$$\frac{I}{I_\odot} = \frac{1}{r^2}\,\frac{2}{3}\,\frac{a^2\ 0.75\ M_T}{\frac{4}{3}\,\pi\,\rho\,a^3} \tag{A-3}$$

Combining equations (A-2) and (A-3),

$$a = \frac{0.75\ M_T\ 10^{-0.4\ (m_\odot - m_v)}}{2\,\pi\,r^2\,\rho} \tag{A-4}$$

For the Apollo 12 dumps, $M_\odot = -26.78$, $r = 1.1 \times 10^{10}$ cm, $M_T = 1.21 \times 10^4$ gm, $\rho = 1$ gm/cm^3, $m_v = 12$;

$a = 0.039$ cm.

For the Apollo 13 dumps, $r = 6.7 \times 10^9$, $M_T = 1.06 \times 10^4$ gm, $m_v = 9$;

$a = 0.0058$ cm.

Therefore, the average particle radius must be between 58 and 390 microns. The difference apparently lies in the observer's ability to estimate the visual magnitude to an accuracy better than 1 magnitude. An average of the two results is 224 microns.

APPENDIX B

Effect of Fogging and Reciprocity Failure on Film Type 2485

In performing photographic photometry on very high speed film that has been exposed to the space environment, the effect of fogging must be considered. Figure 13 shows the D-log E curve for standard 2485 film exposed for 1/100 sec and processed with D-19 chemistry at 85°F for 8 min, 50 sec. The solid lines represent the sensitometry calibration performed by C.L. Ross of the Apollo Photo Science Team on the flight film. For a consistency check, scans were made across corresponding regions of sequential frames taken at 1-sec and 10-sec exposures. The densities measured on the 10-sec frame were plotted against corresponding densities measured on the 1-sec frame. The results are shown in Figure 14. These data were also plotted in Figure 13. The results are consistent with the flight film calibration data.

A similar technique was used to obtain reciprocity data for the 100-sec exposure. Figure 15 is a plot of the measured densities on frames exposed for 100 sec, compared to corresponding points on 10-sec frames. Again, all points seem to fall on a smooth curve except for the points taken from frames seven and eight. Apparently the exposure on one of the frames was in error. The 1-sec exposure in frame six was not above background fog, which indicates that the 10-sec exposure should have a density less than 1.15. Therefore, it seems more likely that the 100-sec exposure was actually exposed longer than 100 sec. Using these data and the 10-sec D-log E curve taken from flight film calibration, the D-log E curve for the 100-sec exposure is constructed in Figure 13.

The reciprocity data are plotted in the standard form in Figure 16. Before the flight film calibration was available, an alternative attempt to obtain reciprocity data was made by the Johnson Space Center photolab by pre-fogging 2485 film to the base fog of the flight film and performing sensitometry for exposure times up to 10 sec. This produced substantially more reciprocity failure, as may be seen by comparing the results in Figure 16 with the flight film results.

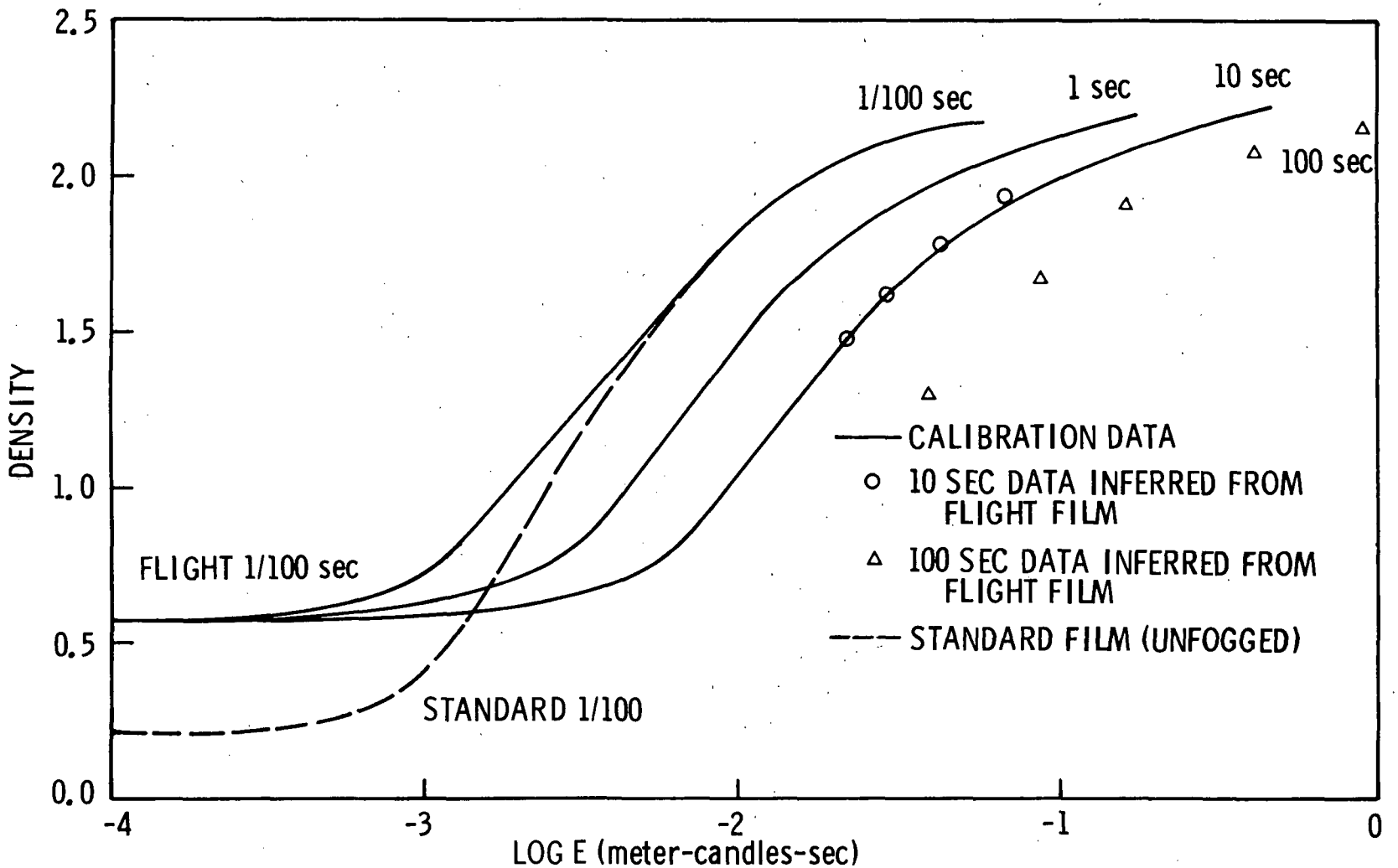

Figure 13. D-log E curves for type 2485 film at different exposure times. The effect of radiation fogging of the flight film is evident.

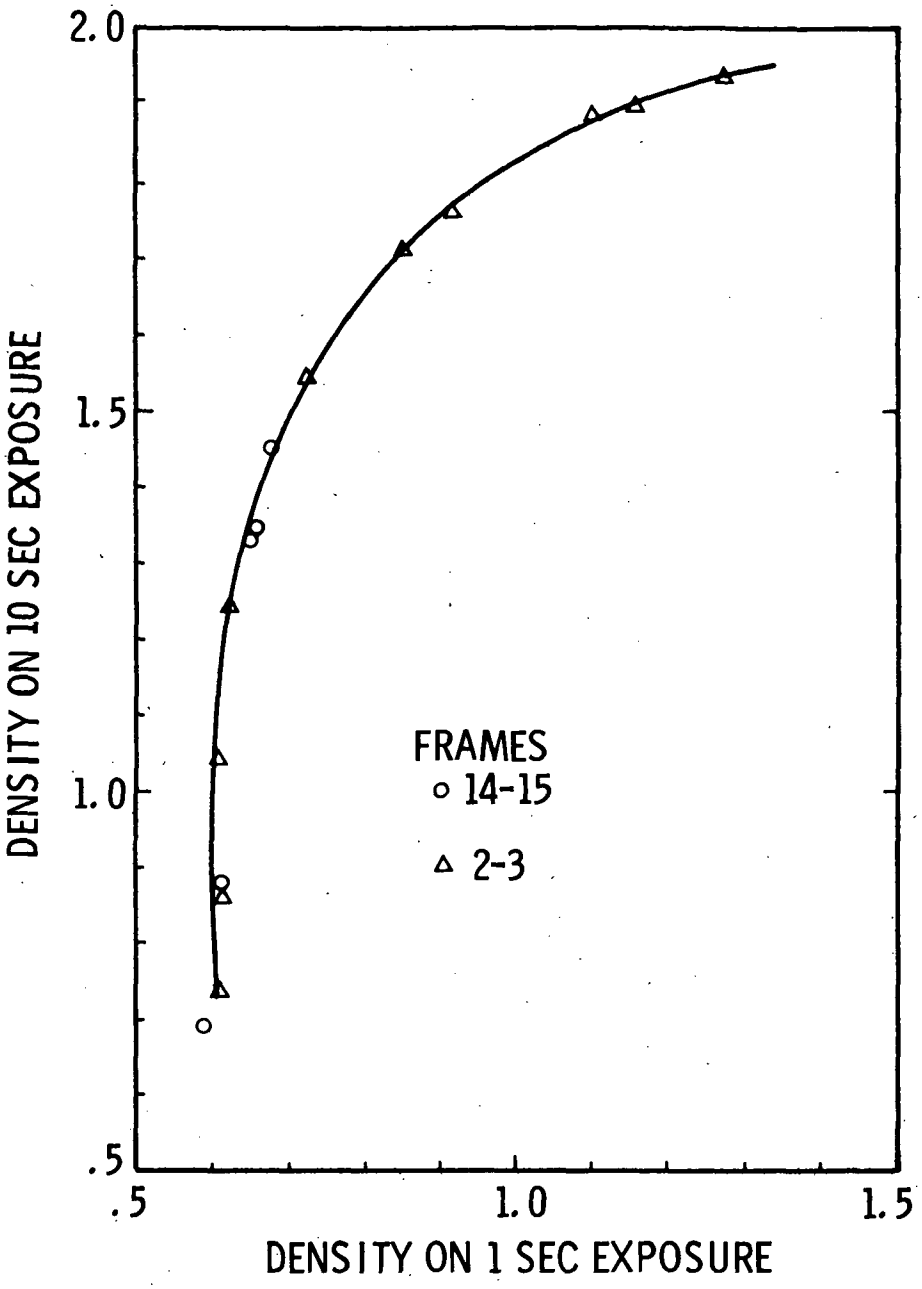

Figure 14. Comparison of densities on frames exposed for 1 sec with identical frames exposed for 10 sec.

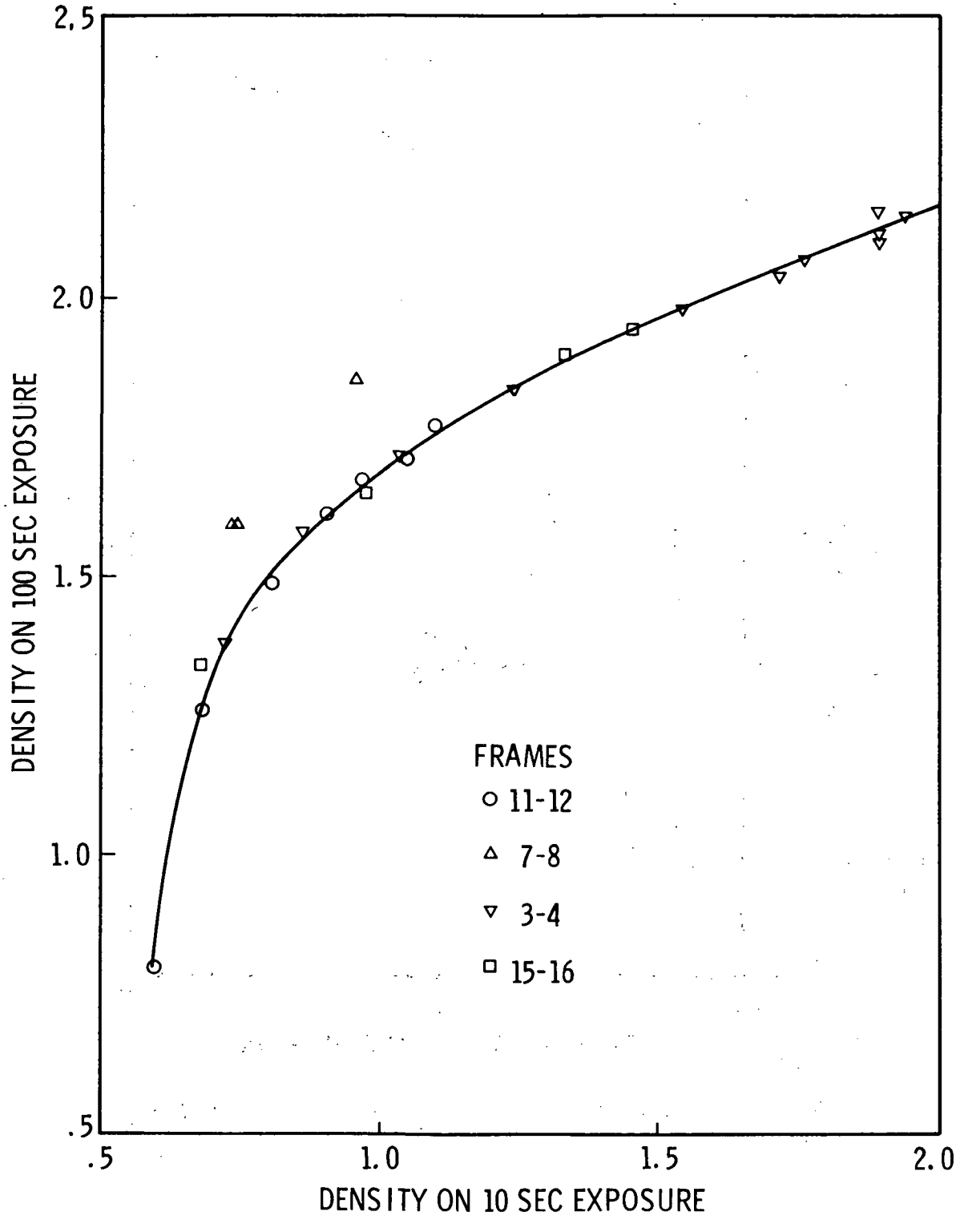

Figure 15. Comparison of densities on frames exposed for 10 sec with identical frames exposed for 100 sec. The anomalous points off frames 7 and 8 apparently result from an error in the exposure time.

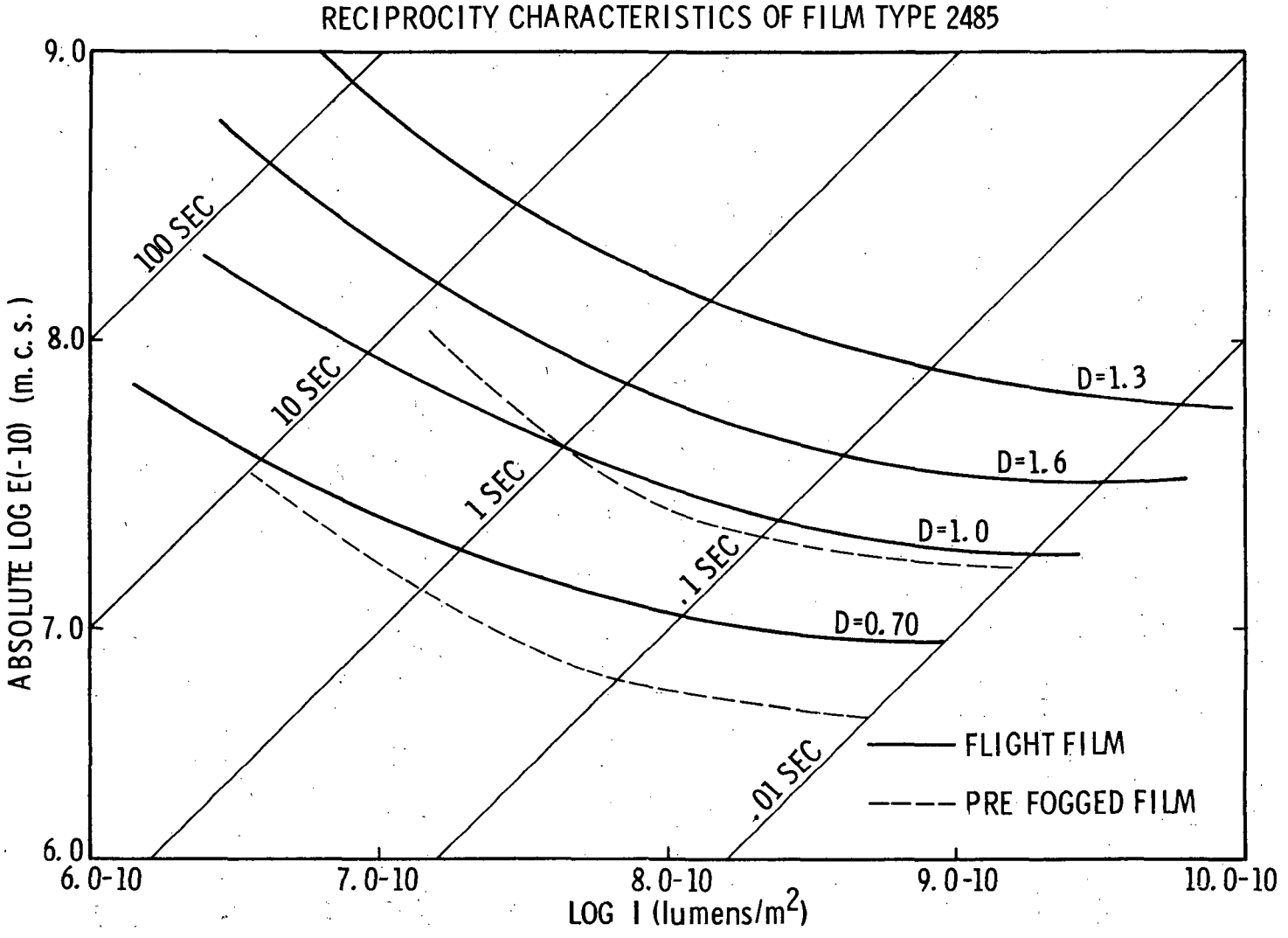

Figure 16. Reciprocity data for type 2485 film fogged by flight radiation to a density of 0.56. Also shown for comparison is film pre-fogged to the density of the flight film. As may be seen, the reciprocity behavior is not the same.

APPENDIX C

Analysis of Scattered Light in Stellar Camera Glare Shield

The stellar camera is suspended below the SIM bay and is oriented with its optical axis 96 deg above the nadir and perpendicular to the vehicle X-axis. The spacecraft shields the camera from the sun except near the terminator. A glare shield with a 45-deg truncation shields against the lunar albedo. However, light from the underneath side of the Service Module will be incident on the open side of the glare shield. A rough order of magnitude analysis of the brightness contribution from this light will be attempted.

If a surface is illuminated by another surface whose brightness is B_0 and that subtends a solid angle ω, the incident intensity is

$$I_i = B_0 \int_{\omega} \cos \theta_i \, d\omega \quad , \tag{C-1}$$

where θ_i is the angle the position vector of each element $d\omega$ of the illuminating surface makes with the illuminated surface. The integral is called the view factor, F_v.

The brightness of the illuminated surface B_i is related to the incident intensity by

$$B_i = I_i F(\theta) \quad , \tag{C-2}$$

where $F(\theta)$ is the phase function, sometimes referred to as the bidirectional reflectance function (BDRF), and has the dimension steradians^{-1}.

For a flat, perfectly diffusing Lambertian surface, the phase function is

$$F(\theta) = \frac{R \cos \theta}{\pi} \quad , \tag{C-3}$$

where θ is the angle between the reflecting surface normal and the reflected ray and R is the albedo.

The brightness of the moon is 2.3×10^{-6} $B_{\odot}$. From the spacecraft altitude the moon subtends approximately 4 steradians. The view factor for an infinite plane is π. Therefore, a rough estimate of the view factor is 2. Treating the underside of the spacecraft as a flat diffuse surface with an albedo of 0.9, the brightness when viewed at angle θ to the normal is

$$B_{sm} = \frac{2\,(0.9)\,B_{\mathbb{Q}}\,\cos\theta}{\pi} \qquad \text{(C-4)}$$

Assume the major contribution of light incident on the glare shield comes from a 30-deg half-angle cone about a line 45 deg to the bottom of the glare shield. The view factor is estimated to be approximately 0.6 and θ is approximately 55 deg. The incident light is, therefore,

$$I_{shield} = 0.2\,B_{\mathbb{Q}}$$

The brightness of the inside of the glare shield at the camera lens is

$$B_{shield} = 0.2\,B_{\mathbb{Q}}\,F(\theta)$$

The inside of the glare shield is painted with 3M Black Velvet antiglare enamel. This paint has an albedo of 0.023 at near normal incidence and reflection. However, for large angles of reflection, the BDRF actually increases instead of following the cosine behavior characteristic of a Lambertian surface. Figure 17 shows measured data for the case of normal incidence and 45-deg incidence. Notice the very large increase in the BDRF at large angles for light incident at -45 deg.

The illuminated portion of the glare shield is estimated to have a view factor of 0.4 and the lens is estimated to be 70 deg from the normal of the illuminated region. The BDRF is, therefore, 0.022 from Figure 17. The intensity incident on the lens is

$$I_{lens} = (0.2)\,(0.022)\,(0.4)\,B_{\mathbb{Q}}$$

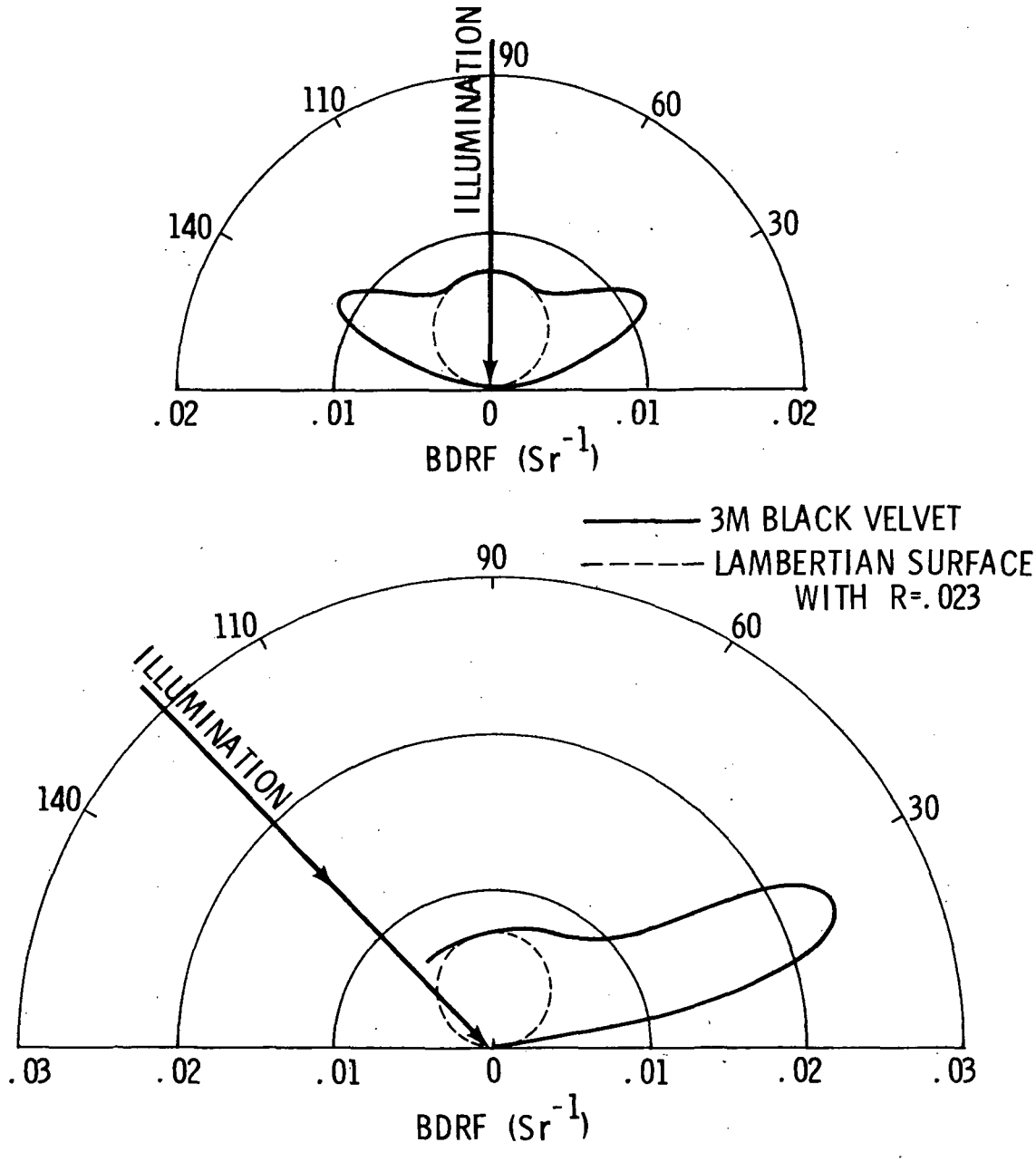

Figure 17. Bidirectional reflectance function (BDRF) (observed brightness divided by normal illuminating intensity) for 3M Black Velvet paint. The BDRF for a white Lambertian surface is $1/\pi$. Black Velvet paint has a normal reflectance of 0.023; however, its scatter function is quite different from a Lambertian surface at large angles, particularly under oblique illumination.

$$I_{lens} = 1.7 \times 10^{-3} B_{\leftmoon}$$

$$I_{lens} = 4.0 \times 10^{-9} B_{\odot}$$

Typical lens BDRF values for off-axis scatter are 0.005 to 0.01 sr^{-1}, depending on the surface, surface cleanliness, etc. The expected glare is, therefore, estimated to be $10^{-10.4}$ to $10^{-10.7}$.

APPENDIX D

Effect of Melting of Ice Crystals on Visibility Criteria

The maximum distance is given by equation (14)

$$R_{max} = \left(\frac{d_\ell^2 \, t_e \, I_\odot}{6 \, A_{film} \, E_f} \right)^{1/2} a \, (R_{max}) \quad , \tag{D-1}$$

but

$$a \, (R_{max}) = a_0 \left(1 - \frac{R_{max}}{R_1} \right) \quad . \tag{D-2}$$

Let

$$\left(\frac{d_\ell^2 \, t_e \, I_\odot}{6 \, A_{film} \, E_f} \right)^{1/2} = C \tag{D-3}$$

and

$$\frac{\rho v}{\dot{m}} = b \quad ; \tag{D-4}$$

therefore

$$R_{max} = \frac{1}{2} \, \frac{bc \, a_0}{b^2 - c^2} \, \left(- c \pm \sqrt{4 \, b^2 - 3c^2} \right) \quad . \tag{D-5}$$

For a case where ρ = 1 gm/cm and $\dot{m}$ = 1.86 X 10^{-6} gm/cm^2/sec, then b = 5.27 X 10^5 v (cm/sec).

For a case where d_ℓ = 0.027, t_e = 1.5 sec, $I_\odot$ = 1.365 X 10^5 lum/m^2, A_{film} = 10^{-9} m^2, and E_f = 0.59 meter-candles-sec, then C = 2.06 X 10^5. Note that for b >> c, $R_{max} \rightarrow c\, a_0$.

If v = 1 cm/sec, then R_{max} = 1.81 X 10^5 a_0; or if v = 10 cm/sec, then R_{max} = 2.02 X 10^5 a_0; or if v $\geqslant$ 100 cm/sec, then R_{max} = 2.06 X 10^5 a_0.

The R_{min} is given by

$$R_{min} = \frac{6\, R_\perp\, v\, F^2\, E_f}{d_\ell\, I_\odot\, a_0^2\, (1 - R_{min}/R_1)^2} \qquad \text{(D-6)}$$

Let

$$\frac{6\, R_\perp\, v\, F^2\, E_f}{d_\ell\, I_\odot\, a_0^2} = R^* \quad , \qquad \text{(D-7)}$$

then

$$R_{min}\, (1 - R_{min}/R_1)^2 = R^* \quad , \qquad \text{(D-8)}$$

which is a cubic to be solved for R_{min}.

The left-hand side is maximized by setting $R_{min} = R_1/3$, which yields 4 R_1/27. If this value is less than R*, the particle melts before it gets in range to be seen. Putting in the various values specified previously,

$$R^* = 1.10 \times 10^{-5}\, v/a_0^2 \quad \text{(all in MKS)} \qquad \text{(D-9)}$$

Therefore,

$$\frac{4}{27}\,\frac{\rho\, v\, a_0}{\dot{m}} \geqslant 1.10 \times 10^{-5}\,\frac{v}{a_0^2} \quad , \tag{D-10}$$

if the particle is to live long enough to become visible.

Solving for a_0,

$$a_0^3 \geqslant 1.10 \times 10^{-5}\,\frac{27\,\dot{m}}{4\,\rho} = \frac{27\,(1.10 \times 10^{-5})\;(1.86 \times 10^{-5}\ \mathrm{kg/m^2/sec})}{4\ 1000\ \mathrm{kb/m^3}} \quad , \tag{D-11}$$

thus

$$a_0 \geqslant 1.11 \times 10^{-4}\ \mathrm{m} \quad ,$$

and

$$a_0 \geqslant 111\ \mu\mathrm{m} \quad .$$

For a_0 greater than this value, the cubic may be readily solved by successive approximations of

$$R_{min}^{i+1} = \frac{R^*}{(1 - R_{min}^{i}/R_1)^2} \quad , \tag{D-12}$$

and convergence is very rapid.

Figure 18 is a plot of R_{max} and R_{min} as a function of a_0 for various velocities. R_{max} is not significantly affected by melting for velocities larger than 10 cm/sec. R_{min} is affected by melting only at particle sizes near a critical value below which particles do not live long enough to become visible. The dashed curves are the values for R_{min} if

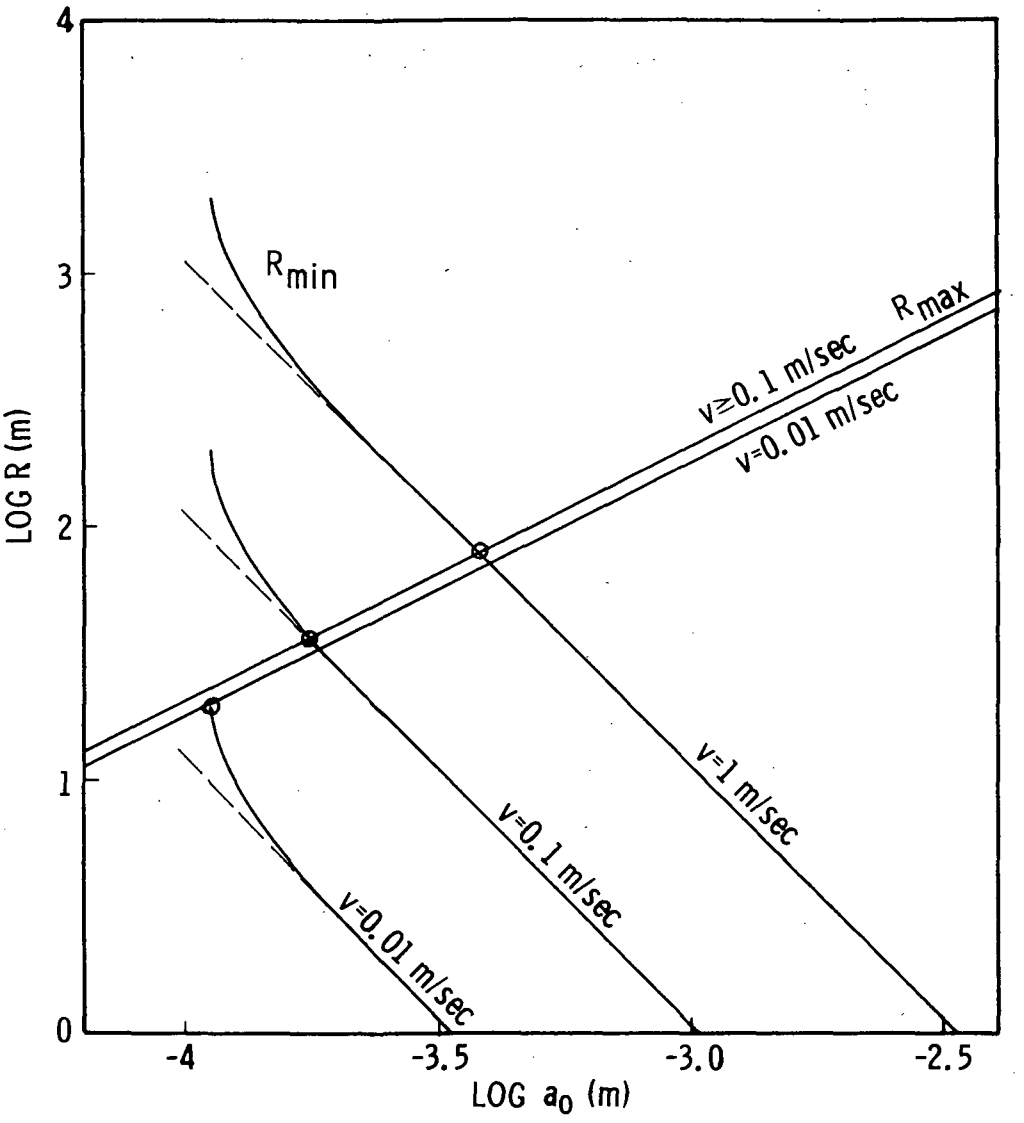

Figure 18. Plot of maximum distance (R_{max}) ice particle may travel while melting before it falls below the detection threshold of the stellar camera and the minimum distance (R_{min}) ice particle must travel before its image size and writing speed allow it to be detected by the stellar camera as a function of initial particle radius. An evaporation rate of 1.86×10^{-6} gm/cm^2/sec was assumed for the evaporation rate. Dashed lines indicate a zero melting rate. In the case of R_{max}, the effect of zero melting is to make R_{max} independent of velocity. Therefore, the dashed line is identical with the curve for $v \geq 0.1$ m/sec. The intersection of R_{min} and R_{max} indicates the minimum size required for a particle to be seen. As may be seen, these intersections are little affected by the effect of melting for velocities of 0.1 m/sec and greater.

melting is not considered. The intersections of R_{min} and R_{max} represent the smallest particle that can be seen at the velocity corresponding to the curves. As may be seen, these intersections are affected only for velocities lower than 0.1 m/sec.

REFERENCES

1. Newkirk, G.N.: The Optical Environment of Manned Spacecraft. Planet & Space Sci 15, 1967, pp. 1267-1285.

2. Kovar, N.S.; Kovar, R.P.; and Bonner, G.P.: Light Scattering by Manned Spacecraft Atmospheres. Planet. Space Sci, 17, 1969, pp. 143-154.

3. Grobman, W.D.; and Buffalano, C.: New Conclusions Concerning the Observation of Faint Sources from a Sunlit Spacecraft. Planet. Space Sci. 17, 1969, pp. 1089-1096.

4. Buffalano, A.C.; Kratage, M.L.; and Sharma, R.D.: Interpretation of Visual Observations of Apollo Water Dumps – Case 340. Bellcomm Memorandum B7107014, July 14, 1971.

5. Naumann, R.J.: Apollo 15 Contamination Photography. NASA TM X-64681, July 5, 1972.

6. Heinisch, R.P.: Study of Visual Detection of Stars in a Spacecraft Environment. Honeywell Doc. 12127, NASA Contract NAS2-5015, April 1969.

7. Fastie, W.G., et. al.: Ultraviolet Spectrometer Experiment. Apollo 17 Preliminary Science Report, NASA SP-330, 1973, p. 23-1.

8. Hoffman, J.H.; Hodges, R.R.; and Evans, D.E.: Lunar Orbital Mass Spectrometer Experiment. Apollo 15 Preliminary Science Report, NASA SP-289, p. 19-1.

9. West, W.S.; Gore, J.V.; Kasha, M.A.; and Bilsky, H.W.: Spacecraft Charge Buildup Analysis. NASA SP-276, 1971.

10. Naumann, R.J.: Dynamics and Column Densities of Small Particles Ejected from Spacecraft. NASA TN D-7590, Feb 1974.

11. Roman, N., Chairman: Final Report of the Payload Planning Working Groups. Vol. 1, Astronomy, NASA Goddard Space Flight Center, Greenbelt, Md., May 1973.

NASA-Langley, 1974

"The aeronautical and space activities of the United States shall be conducted so as to contribute . . . to the expansion of human knowledge of phenomena in the atmosphere and space. The Administration shall provide for the widest practicable and appropriate dissemination of information concerning its activities and the results thereof."

—NATIONAL AERONAUTICS AND SPACE ACT OF 1958

NASA SCIENTIFIC AND TECHNICAL PUBLICATIONS

TECHNICAL REPORTS: Scientific and technical information considered important, complete, and a lasting contribution to existing knowledge.

TECHNICAL NOTES: Information less broad in scope but nevertheless of importance as a contribution to existing knowledge.

TECHNICAL MEMORANDUMS: Information receiving limited distribution because of preliminary data, security classification, or other reasons. Also includes conference proceedings with either limited or unlimited distribution.

CONTRACTOR REPORTS: Scientific and technical information generated under a NASA contract or grant and considered an important contribution to existing knowledge.

TECHNICAL TRANSLATIONS: Information published in a foreign language considered to merit NASA distribution in English.

SPECIAL PUBLICATIONS: Information derived from or of value to NASA activities. Publications include final reports of major projects, monographs, data compilations, handbooks, sourcebooks, and special bibliographies.

TECHNOLOGY UTILIZATION PUBLICATIONS: Information on technology used by NASA that may be of particular interest in commercial and other non-aerospace applications. Publications include Tech Briefs, Technology Utilization Reports and Technology Surveys.

Details on the availability of these publications may be obtained from:

SCIENTIFIC AND TECHNICAL INFORMATION OFFICE

NATIONAL AERONAUTICS AND SPACE ADMINISTRATION

Washington, D.C. 20546